South Dakota State University

Open PRAIRIE: Open Public Research Access Institutional Repository and Information Exchange

Electronic Theses and Dissertations

2020

Applications of Hydrodynamic Cavitation in Dairy Manufacturing: Process Development and Standardization

Jae Young Sim
South Dakota State University

Follow this and additional works at: https://openprairie.sdstate.edu/etd

 Part of the Dairy Science Commons, and the Food Microbiology Commons

Recommended Citation

Sim, Jae Young, "Applications of Hydrodynamic Cavitation in Dairy Manufacturing: Process Development and Standardization" (2020). *Electronic Theses and Dissertations*. 3940.
https://openprairie.sdstate.edu/etd/3940

This Thesis - Open Access is brought to you for free and open access by Open PRAIRIE: Open Public Research Access Institutional Repository and Information Exchange. It has been accepted for inclusion in Electronic Theses and Dissertations by an authorized administrator of Open PRAIRIE: Open Public Research Access Institutional Repository and Information Exchange. For more information, please contact michael.biondo@sdstate.edu.

APPLICATIONS OF HYDRODYNAMIC CAVITATION IN DAIRY MANUFACTURING: PROCESS DEVELOPMENT AND STANDARDIZATION

BY

JAE YOUNG SIM

A thesis submitted in partial fulfilment of the requirement for the

Master of Science

Major in Biological Sciences

Specialization in Dairy Science

South Dakota State University

2020

THESIS ACCEPTANCE PAGE

JaeYoung Sim

This thesis is approved as a creditable and independent investigation by a candidate for the master's degree and is acceptable for meeting the thesis requirements for this degree. Acceptance of this does not imply that the conclusions reached by the candidate are necessarily the conclusions of the major department.

Sergio Martinez Monteagudo
Advisor Date

Vikram Mistry
Department Head Date

Dean, Graduate School Date

I dedicate this thesis to my family who support and encourage me to grow as a food science researcher. My father Ki Sub Shim, My mother Kyung Ja Park, and my brother Jae Kwang Shim. Thank you for your support and trust in me.

ACKNOWLEDGEMENTS

I would like to express my sincere appreciation to my advisor Sergio I. Martinez-Monteagudo. He gave me the opportunity to join his research team and guided me during my research project. He understood my curiosity of various areas and created the projects that I was able to enjoy and learn more from. One of the best times during my master's program was research discussions with my advisor. He accepted different points of view and he treated me as a scientist rather than only a student. Also his advice for the scientific presentation was helpful and allowed me to improve my speech Thank you for your support.

I would also like to thank Dr. Sanjeev Anand who shared his microbiology knowledge in this research project. His helping and teaching allowed me to achieve the research results in a short time. I also acknowledge the people in the Davis diary plant who helped my research trials. John Haberkorn, dairy plant manager, thanks for sharing the products made from the SDSU dairy plant. Steven Beckman, R&D manager, he also shared his engineering knowledge with me, and troubleshooting the issue with hydrodynamic cavitation was a huge help for me and I do appreciate it and respect him. Howard Bonnemann who shared his ice cream knowledge and working experience at the ice cream plant helped me to accomplish my ice cream research project. I would like to thank the rest of my committee members, Dr. Vikram Mistry and Dr. Thomas Stenvig. Special Thank you to Dr. Tom E. Schumacher. He always shares his time with me and provides not only academic assistance but also life lessons and advice. I also thank my family and my friends who care about me and are a positive influence for me.

This work has been made possible through the financial support of Dairy Management Inc., and partial support from USDA National Institute for Food and Agriculture (HATCH project SD00H607-16).

TABLE OF CONTENTS

LIST OF TABLES

LIST OF FIGURES

LIST OF EQUATIONS

ABBREVIATIONS

C	Heat capacity of the liquid (J kg^{-1} °C^{-1})
C_{in}	Cavitation inception (dimensionless)
C_{pmin}	Minimum pressure coefficient (dimensionless)
C_p	Pressure coefficient (dimensionless)
C_v	Cavitation number (dimensionless)
D_H	Diameter of the housing (m)
D_r	Diameter of the rotor (m)
G	Gap width between the rotor and the stator (m)
H	Thermal energy generated due to cavitation (kJ)
HC	Hydrodynamic cavitation
H_{ind}	Height of the indentations within the rotor (m)
HTST	High-Temperature-Short-Time
ICM	Ice cream mix
LVE	Linear viscoelastic region
n_{ind}	Number of indents
N_r	Speed of the rotor (RPS)
N_Q	Corresponding flow number (dimensionless)
p_1	Inlet pressure (Pa)
p_2	Outlet pressure (Pa)
p_{app}	Pressure at which cavitation first appear (Pa)
p_v	Water vapor pressure (Pa)

Q	Flow rate (L h^{-1})
r	Pressure ratio (dimensionless)
R_e	Reynolds number (dimensionless)
SMC	Skim milk concentrate
UC	Ultrasonic cavitation
UHT	Ultra-High-Temperature
v_c	Velocity required for cavitation (m s^{-1})
v_{gap}	Velocity of the liquid at gap (m s^{-1})
v_r	Velocity at the surface of the rotor (m s^{-1})
W_r	Width of the rotor (m)
W_{ind}	Width of the indentations within the rotor (m)

Variables

ΔT_c	Temperature gradient generated due to cavitation (°C)
ρ	Density of the liquid (kg m^{-3})
μ	Kinematic viscosity (m^2 s^{-1})
ω	Angular velocity

ABSTRACT

APPLICATIONS OF HYDRODYNAMIC CAVITATION IN DAIRY MANUFACTURING: PROCESS DEVELOPMENT AND STANDARDIZATION

JAE YOUNG SIM

2020

The phenomenon of hydrodynamic cavitation involves the formation, growth, and subsequent collapse of bubbles when a given liquid experienced a reduction of pressure below its vapor pressure. The presence of cavitation limits the performance and the safe operation of many machinery and pumps. However, innovation in the design of the hydrodynamic cavitation devices has offered promising applications in the food and dairy industry. Upon collapse of the cavities, the fluid experiences significant mechanical effects (shear and turbulence) as well as instantaneously elevation of the fluid temperature. All these effects can be put to work for mixing, dispersion, particle size reduction, disinfection, and emulsification. In this thesis, the feasibility of using a rotational cavitator for different unit operations was systematic evaluated. The feasibility of hydrodynamic cavitation was evaluated in terms of analysis of cavitation parameters, characterization of the increase in the fluid temperature, microbial efficiency, and emulsification of ice cream mix. The analysis of the cavitator revealed that the velocities generated inside the rotational cavitator are sufficiently high to induce cavitation within the fluid. The development of the cavitation was influenced by the flow rate, speed of the rotor, temperature, and fluid properties. The pressure at which cavitation would first appear was calculated as a function of the operating parameters. The increase in the temperature of the fluid was modeled, showing satisfactory correlation with the

experimental data. The increased in the temperature of the fluid due to cavitation was used to develope a process for assisting thermal pasteurization with the idea of reducing the log counts of thermoduric bacteria. The newly developed process can be operated within a wide range of processing conditions (50-300 L h^{-1}, 600-3600 RPM, 70-85°C with residence time from 10-110 s). It was found a 3.5 log reduction of *Bacillus coagulans* by cavitation followed by thermal treatment, while thermal treatment along yielded a 2.77 log reduction. The hydrodynamic cavitation was applied during the manufacture of ice cream with the idea of reducing the concentration of stabilizers. Particle size of ice cream mix and rheology test was conducted to determine the influence of the stabilizer amounts in ice cream mix. Hydrodynamic cavitation itself reduced the particle size of cream and ice cream mix. Dynamic rheological measurements (strain and frequency sweeps) of ICM indicated increased product stability at a rotation speed of 3600 RPM and flow of 100 L $^{-1}$. However, the mechanical spectra were considerable different. Imparted viscosities at medium shear rates were at least 2-fold greater compared to formulations homogenized conventionally.

Chapter 1

Introduction and objectives

1.1. Significance of the research

Consumers through social media have begun to redefine the desired attributes of food and dairy products. Nowadays, the assurance of microbial safety is no longer sufficient to meet the new standards of modern consumers. Instead, the perception among the consumers regarding “healthy” and “unhealthy” ingredients has driven the dairy industry to reformulate their existing portfolio of products with perceived healthy ingredients and free of unfamiliar compounds (Asioli et al., 2017).

Around the globe, scientists and engineers have been developing and implementing emerging technologies in response to consumers' interest in healthy processed foods. High-pressure processing, high-pressure homogenization, pulsed electric fields, ultrasound, and cold-plasma are examples of such technologies. The advantages and disadvantages of these technologies have been reviewed comprehensibly elsewhere (Zhang et al., 2011; Balasubramaniam, Martínez-Monteagudo, & Gupta, 2015; Martínez-Monteagudo, Yan, Balasubramaniam, 2017).

Research concerning emerging technologies conducted in universities, national laboratories, and industries have shown several promises in the modification of physical and chemical properties of foods. All these developments have led to a number of applications, from pasteurization and extension of shelf-life to extraction of bioactive components. Nowadays, microbial safety can be achieved by creative combinations of

different lethal agents that result in a reduced impact on nutritional properties. However, the effect of such practices on the dispersion of the structural elements (particles, molecules, globules, droplets, aggregates, granules, etc.) has been somewhat overlooked. In this area, the work developed in this thesis aims at studying hydrodynamic cavitation (HC), a novel technology. HC consists of a stationary cylinder and a high-speed rotating inner cylinder with indentations (Carpenter et al., 2017). Due to the high-speed of the inner cylinder, cavities are formed and subsequently collapsed, releasing waves of energy (Milly et al., 2007; Milly et al., 2008). Depending on the conditions, the fluid experiences high shear, cavitation, and turbulence (Badve, Bhagat, & Pandit, 2015). Such mechanical effects are put to work for mixing, dispersion, particle size reduction, and emulsification. The specific objectives were to:

- Perform engineering analysis of the hydrodynamic cavitation using selected cavitation parameters (Chapter 2).
- Characterize the rise in temperature as a function of the processing conditions (Chapter 2).
- Design and build the cavitation processing (Chapter 3).
- Evaluate the inactivation of thermoduric microorganisms (Chapter 3).
- Evaluate the effect of hydrodynamic cavitation on the particle size distribution of the ice-cream mix (Chapter 4).
- Evaluate the effect of hydrodynamic cavitation on the rheological behavior of the ice-cream mix (Chapter 4).

1.2. References

Asioli, D., Aschemann-Witzel, J., Caputo, V., Vecchio, R., Annunziata, A., Næs, T., & Varela, P. (2017). Making sense of the "clean label" trends: A review of consumer food choice behavior and discussion of industry implications. Food Research International, 99:58-71.

Badve, M. P., Bhagat, M. N., & Pandit, A. B. (2015). Microbial disinfection of seawater using hydrodynamic cavitation. Separation and Purification Technology, 151:31-38.

Balasubramaniam, V. B., Martínez-Monteagudo, S. I., & Gupta, R. (2015). Principles and application of high pressure–based technologies in the food industry. Annual Reviews of Food Science and Technology, 17(6):435-462.

Carpenter, J., Badve, M., Rajoriya, S., George, S., Saharan, V. K., & Pandit, A. B. (2017). Hydrodynamic cavitation: an emerging technology for the intensification of various chemical and physical processes in a chemical process industry. Reviews in Chemical Engineering, 33(5):433-468.

Martínez-Monteagudo, S. I., Yan, B., & Balasubramaniam, V. M. (2017). Engineering process characterization of high-pressure homogenization—from laboratory to industrial scale. Food Engineering Reviews, 9(3):143-169.

Milly, P. J., Toledo, R. T., Harrison, M. A., & Armstead, D. (2007). Inactivation of food spoilage microorganisms by hydrodynamic cavitation to achieve pasteurization and sterilization of fluid foods. Journal of food science, 72(9):M414-M422.

Milly, P. J., Toledo, R. T., Kerr, W. L., & Armstead, D. (2008). Hydrodynamic cavitation: characterization of a novel design with energy considerations for the

inactivation of Saccharomyces cerevisiae in apple juice. Journal of food science, 73(6):M298-M303.

Zhang, H., Barbosa-Canovas, G.V., Balasubramaniam, V. M., Dunne, C. P., Farkas, D.F., & Yuan, J. T. C. (2011). Nonthermal Processing Technologies for Food. Oxford, UK:Wiley-Blackwell

Chapter 2.

Analysis of the hydrodynamic cavitation

2. 1. Introduction

The term cavitation refers to the phenomenon of formation of cavities or bubbles within a liquid, their growth, and subsequent collapse when the pressure of the liquid is suddenly reduced below its vapor pressure (Carlton, 2012). The phenomenon of cavitation was first observed in 1894 through the damage on the propeller of sailing ships (Kim et al., 2019). Cavitation is responsible for issues such as erosion (Ahmed, 1998), noise, and vibration (Petkovšek & Dular, 2013), which may lead to malfunction of a number of machinery and pumps. Extensive research has been conducted on the fundamentals of cavitation in order to minimize the wear and damage in machinery (Ahmed, 1998; Petkovšek & Dular, 2013; Jian et al., 2015). In dairy manufacturing, the collapse of the bubbles on metal surfaces causes localized stresses of high amplitude, wearing the surfaces of homogenizer and pumps (Innings et al., 2011).

The underlying physics of the formation of cavitation is based on the pressure-volume relationship of the van der Waals equation (Endo, 1994), which states that within the transition from liquid to vapor, there is an interphase where both phases coexist, which corresponds to the length of the spinodal line of stability of the liquid. Cavitation occurs only when enough nuclei become unstable and grow when subjected to a pressure reduction. The internal forces, produced by the partial pressures of the gas and vapor within the nucleus, must be balanced by the ambient pressure and the surface-tension pressure at the nucleus-liquid interface (Chahine, 1997). The growth of the cavity is

somewhat similar to the evaporation process, where latent heat is supplied from the surrounding. Concomitantly, the temperature of the liquid slightly drops, causing a drop of the vapor pressure of the liquid (Petkovšek & Dular, 2017). Collapsing mechanisms of cavitation bubbles have been reviewed elsewhere (van Wijngaarden, 2016). In general, the collapse of the cavitation bubbles occurs within a very short time span (milli- or micro-seconds), resulting in shockwaves that raise the liquid temperature.

Cavitation is classified according to the method causing the drop in the vapor pressure of the liquid, ultrasonic cavitation (UC) and hydrodynamic cavitation. Arrojo & Benito (2008) comprehensively examined the differences between UC and HC. The pressure pulses derived from HC are quantitatively and qualitatively different from those obtained in UC. The application of sound waves of high-frequency (>20 kHz) results in the formation of bubbles, which forcibly collapse due to the contraction and expansion of the molecules. In UC, the operating frequency and intensity of the ultrasound determine the wave of the spreading pressure within a static liquid. Thus, the pressure pulse is readily controlled in a typical experiment involving ultrasound. Contrary, HC takes place by varying the cross-sectional area of the flow path, which drops the pressure of the fluid. The pulses of pressure experienced in HC are much more complex to characterize since it involves a moving liquid with changing velocity.

Over the last decade, significant progress has been made in the fundamental understanding of the hydrodynamic cavitation (Gogate & Pandit, 2000; Gogate & Pandit, 2005; Arrojo & Benito, 2008; Badve, Bhagat, & Pandit, 2015). In summary, the intensity

of HC is lower than the one experienced in UC, and the dynamics of HC depends on the flow conditions, flow rate, design and geometry of the experimental apparatus (Kumar & Pandit, 1999; Šarc et al., 2017; Badve, Bhagat, & Pandit, 2015).

Recently, innovation in the design of the hydrodynamic cavitation devices has offered promising applications in the food and dairy industry, where the released energy during the cavitation is put to work for disinfection, hydrolysis, mixing, dispersion, emulsification, and particle size reduction. A number of HC devices has been developed based on venturi (Stoop, Bakker, & Kramer, 2015), swirling jet (Mancuso, Langone, & Andreottola, 2017), orifice plate (Habashi et al., 2016), rotor-stator (Patil et al., 2016), and two rotating disc systems (Petkovšek et al., 2013).

Among the HC devices, the rotational device from SPX Flow Technology has shown to enhance drying efficiency of high solids (Li et al., 2018), improve the surface hydrophobicity of soy protein isolate (Li et al., 2020), and reduce the viscosity of concentrated protein solutions (Gregersen et al., 2019). The rotational HC from SPX Flow Technology is a fluid machine that consists of a stationary cylinder and a high-speed rotating inner cylinder with indentations. A schematic representation of the rotational hydrodynamic cavitation apparatus is presented in **Figure 1**. The liquid inside the rotational HC is subjected to a constant change of the cross-sectional area due to the rotation, and consequently the molecules contract and expand periodically, resulting in a high cavitation intensity (Šarc et al., 2018). The majority of the research in relation to rotational HC have focused on identify potential applications, while the fundamental

understanding continues to be largely unknown. In this chapter, the rotational HC is analyzed in terms of cavitation parameters and thermal energy generated as a function of operating parameters (flow rate, speed of the rotor, and fluid properties).

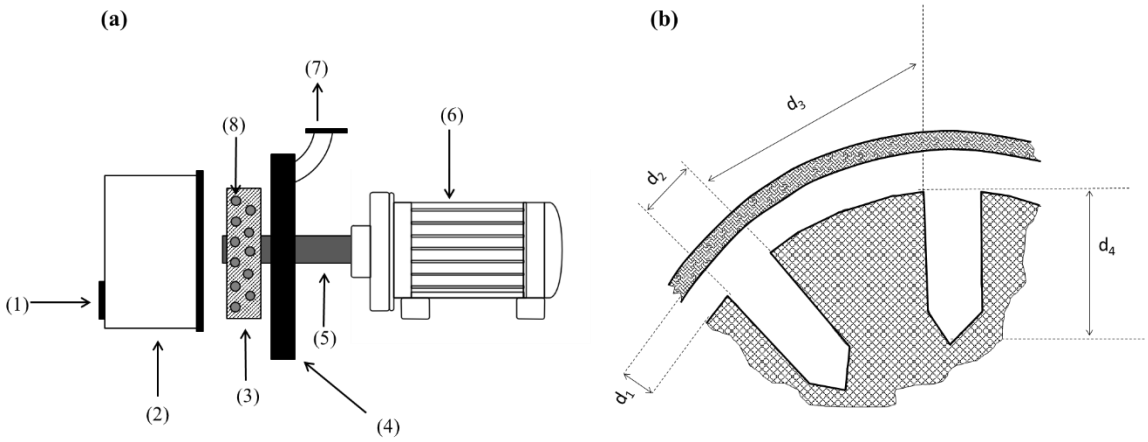

Figure 1. Schematic representation of the hydrodynamic cavitation: (a) assembly of the hydrodynamic cavitator, and (b) schematic view of the indentations inside the housing or stator cylinder. (1) product inlet; (2) housing; (3) rotor; (4) back plate; (5) shaft; (6) rotor; (7) product outlet; (8) indents; d_1 distance between rotor and housing; d_2 diameter of the indents; d_3 distance between indents; and d_4 length of indent. Drawings do not represent real scale.

2. 2. Materials and methods

Rotational hydrodynamic cavitation

The rotational HC from SPX Flow Technology was used for the analysis of the hydrodynamic cavitation. The device consists of a stationary cylinder (housing) and an inner cylinder (rotor) with indentations. The inner cylinder rotates at relatively high speeds (up to 3600 RPM) driven by a mechanical shaft that is coupled to a motor (**Figure 1a**). The inner cylinder consists of 88 indentations equidistantly located around the circumference, and they have cylindrical shaped dead-end bores (**Figure 1b**). A detailed description of the different hydrodynamic cavitation arrangements can be found elsewhere (League & Parker, 2009; Griggs, 2015).

Experimental setup

The test facility of the rotational hydrodynamic cavitation is shown in **Figure 2**. The experimental setup mainly included a feeding tank (20 L), a positive displacement pump (Baldor-Reliance, Fort Smith, AR), a return line, a rotational HC (APV Cavitator, SPX Flow Technology, Crawley West Sussex, United Kingdom), a set of diaphragm valves (Type 3233, Burkert Fluid Control Systems, Huntersville, NC), a set of K-type thermocouples connected to a data logger (Omega Engineering Inc., Stamford, CT), a set of pressure transmitter (Type 405052, JUMO Process Control Inc., East Syracuse, NY), and an electromagnetic flow meter (Siemens MAG 5000, Flow Instruments, Nordborg, Denmark). The rotor was a solid cylinder attached to a gear assembly which was connected to a variable frequency drive that controlled the speed of rotation. The return line (number (3) in **Figure 2**) helps to maintain a constant inlet pressure of about 1.0 bar. The analysis of the rotational cavitator was carried out using tap water, and the whole system was operated under open-loop circuit, where the effluent was only treated once without recirculation. A data acquisition system (PowerFlex® 70, Allen-Bradley by Rockwell Automation, Omaha, NE) was used to record the inlet and outlet temperature and pressure.

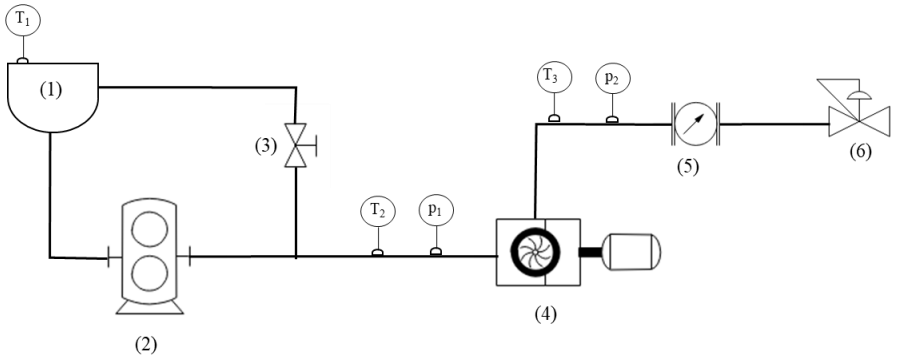

Figure 2. Schematic diagram of the rotational hydrodynamic cavitation setup. (1) feeding tank, (2) positive displacement pump, (3) manually operated diaphragm valve; (4) APV Cavitator; (5) electromagnetic flow meter; and (6) diaphragm valve.

Velocities within the rotational cavitator

The hydrodynamic cavitation described in **Figure 1** resembles that of high-speed homogenizer, where an impeller rotates inside a cage-like stator containing numerous indents. Three main velocities can be derived from the schematic presented in **Figure 1**, including the velocity at the gap (v_{gap}) between the rotor and stator, velocity at the surface of the rotor (v_r), and the required velocity for cavitation (v_c). The gap between the stator and the rotor is somewhat analogous to the throat of a venturi, where the liquid is forced to flow from the indentation through the gap with every turn of the rotor. Such analogy allows to calculate the velocity of the liquid at the moving through the indentation into the gap between the rotor and the stator (v_{gap}) using the corresponding flow number (N_Q) of the rotor proposed by Sano & Usui (1985).

Equation (1)

$$N_Q = 1.3 \cdot \left(\frac{D_r}{D_H}\right)^{-0.86} \cdot \left(\frac{W_r}{D_H}\right)^{0.82} \cdot n_{ind}^{0.6}$$

Where D_r is the diameter of the rotor, D_H is the diameter of the housing or stator, W_r is the width of the rotor, and n_{ind} is the number of indents. The resulting fluid velocity moving through the indentations into the gap between the rotor and the stator can be estimated by Equation (2).

Equation (2)

$$v_{gap} = \frac{N_Q \cdot N_r \cdot D_r^3}{n_{ind} \cdot H_{ind} \cdot W_{ind}}$$

Where N_r is the speed of the rotor, H_{ind} and W_{ind} are the height and width of the indentations within the rotor, respectively. The velocity of the liquid on the surface of rotor was calculated using the angular velocity (ω) (Equation (3)), while the cavitation velocity was obtained using Equation (4).

Equation (3)

$$v_r = r_r \cdot \omega$$

Equation (4)

$$v_c = \sqrt{\frac{p_1 - p_v}{1/2 \cdot \rho}}$$

The flow regime within the rotational cavitator was characterized by the Reynolds number (R_e), which depends on the speed of the rotor (N_r) and geometry of the cavitator according to Equation (5) (Badve et al., 2015).

Equation (5)

$$R_e = \frac{N_r \cdot G^2}{4 \cdot \mu}$$

Where G is the gap width between the rotor and the stator, and μ is the kinematic viscosity.

Cavitation parameters

The analysis of the HC was performed by the calculation of pressure coefficient (C_p), minimum pressure coefficient (C_{pmin}), cavitation appearance (p_{app}), cavitation number (C_v), cavitation inception (C_{in}), and pressure ratio (r).

Equation (6)

$$C_p = \frac{p_1 - p_2}{{}^1\!/_2 \cdot \rho \cdot v_{ind}^2}$$

Equation (7)

$$C_{pmin} = \frac{p_{min} - p_2}{{}^1\!/_2 \cdot \rho \cdot v_{ind}^2}$$

Equation (8)

$$p_{app} = p_v + {}^1\!/_2 \cdot \rho \cdot v_{ind}^2 \cdot \left(-C_{pmin}\right)$$

Equation (9)

$$C_v = \frac{p_2 - p_1}{{}^1\!/_2 \cdot \rho \cdot v_{ind}^2}$$

Equation (10)

$$C_{in} = \frac{p_{app} - p_v}{{}^1\!/_2 \cdot \rho \cdot v_{ind}^2}$$

Equation (11)

$$r = \frac{p_1}{p_2}$$

Thermal energy due to hydrodynamic cavitation

The heat generated or thermal energy (H) due to hydrodynamic cavitation was quantified as the heat generation rate ($\dot{H}$), according to Equation (12) and Equation (13):

Equation (12)

$$\dot{H} = \rho \cdot Q \cdot C \cdot \Delta T_c$$

Equation (13)

$$H = \dot{H} \cdot t$$

where ρ is the density of the liquid (kg m^{-3}), Q is the flow rate (L h^{-1}), C is the heat capacity of the liquid (J kg^{-1} °C^{-1}), ΔT_c is the temperature gradient generated due to cavitation (°C); t is the time, which was arbitrarily set to 100 s. The increase in the product temperature due to cavitation was obtained by measuring the temperature before and after cavitation using K-type thermocouples connected to a data logger.

Temperature increase due to cavitation

A factorial design with three variables (flow rate, speed of the rotor, and total solids) at three levels for each variable (100, 200, and 300 L h^{-1}, 2400, 3000, and 3600 RPM, and 11, 24, and 36%, respectively) was used to studied the effect of variables on the product temperature. Skim milk was concentrated using a falling film evaporator located at the Davis Dairy Plant at South Dakota State University. Briefly, the skim milk was feed into the evaporator at 80°C, and after four-passes the skim milk was concentrated at 36 ± 2% total solids. The samples containing 24% of total solids were obtained by adding water

accordingly. The ΔT_c in water was also evaluated and used as a reference point. Each set of experiments consisted of 15 L of skim milk concentrate, and all experiments were performed in triplicate. The experimental data (ΔT_c) were fitted into a polynomial equation through non-linear regression analysis using the software package Design-Expert version 7.0 (Stat-Ease, Inc. Minneapolis, MN). All graphs were generated using Sigmaplot software V11 for Windows (SPSS Inc., Chicago, IL, USA).

2.3. Results and discussion

Analysis of fluid velocities

Figure 3 shows the velocities considered for the analysis of the rotational cavitator. Overall, the speed of the rotor significantly influenced the magnitude of the velocity at the surface of the rotor, the velocity entering the gap, and the velocity required for cavitation. The surface and gap velocity increased linearly with increasing the rotation speed, reaching values up to 40 and 81 m s^{-1} at 3600 RPM, respectively. Badve et al. (2015) reported similar velocities at the surface of the rotor (18-30 m s^{-1}) in a rotational cavitator (1800-2800 RPM). Contrary, the velocity at which cavitation would appear decreased from 14 to 12 m s^{1} with the rotation speed. The velocities generated inside the rotational cavitator (v_{gap} and v_r) were sufficiently high to induce cavitation within the fluid. Interestingly, the velocities generated inside the cavitator were much higher than the velocity entering the cavitator that ranges from 0.17 to 1.0 m s^{-1}, increasing with the flow rate. Thus, the contribution towards the development of cavitation of the velocity entering the stator is rather negligible, and the main factor affecting the development of cavitation is the speed of the rotor.

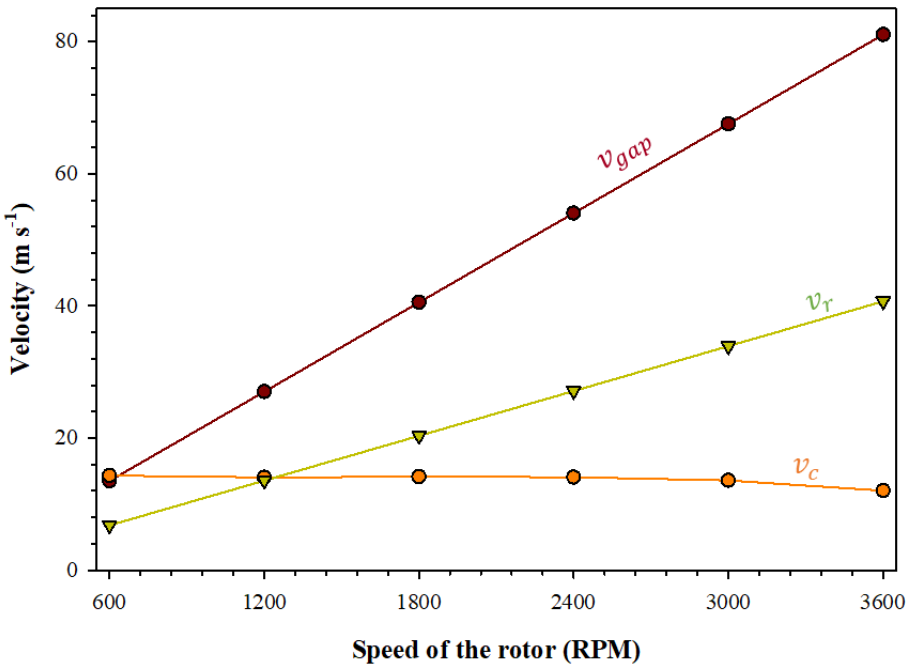

Figure 3. Effect of rotation speed on the gap, surface, and cavitation velocity. v_{gap} is the gap velocity; v_r is the surface velocity generated by the rotor; and v_c is the velocity at which cavitation would appear.

Figure 4 shows the effect of the speed of the rotor and the volumetric flow rate on the Reynolds number. In general, the values of the Reynolds number display an exponential curvature with increasing the speed of the rotor. At 50 L h^{-1}, the Reynolds number varied from 190 to 3,000 when the speed of the rotor increased from 600 and 3600 RPM. Similar behavior, but less pronounced, was observed in the Reynolds number at higher volumetric flow rates when the obtained Reynolds number was 2,368, 1,754, and 1536 at 3,600 RPM for 100, 200, and 300 L h^{-1}, respectively. The Reynolds number can be defined as the ratio of inertial forces to the viscous forces, and its numerical value is of technological interest for a number of applications, including thermal treatment, emulsification, dispersion, and mixing. Interestingly, the majority of the experimental

conditions resulted in fluid conditions under laminar regime ($R_e < 2{,}000$), while only few conditions (low values of volumetric flow rate and high values of speed of rotor) yielded fluid conditions under turbulent regime.

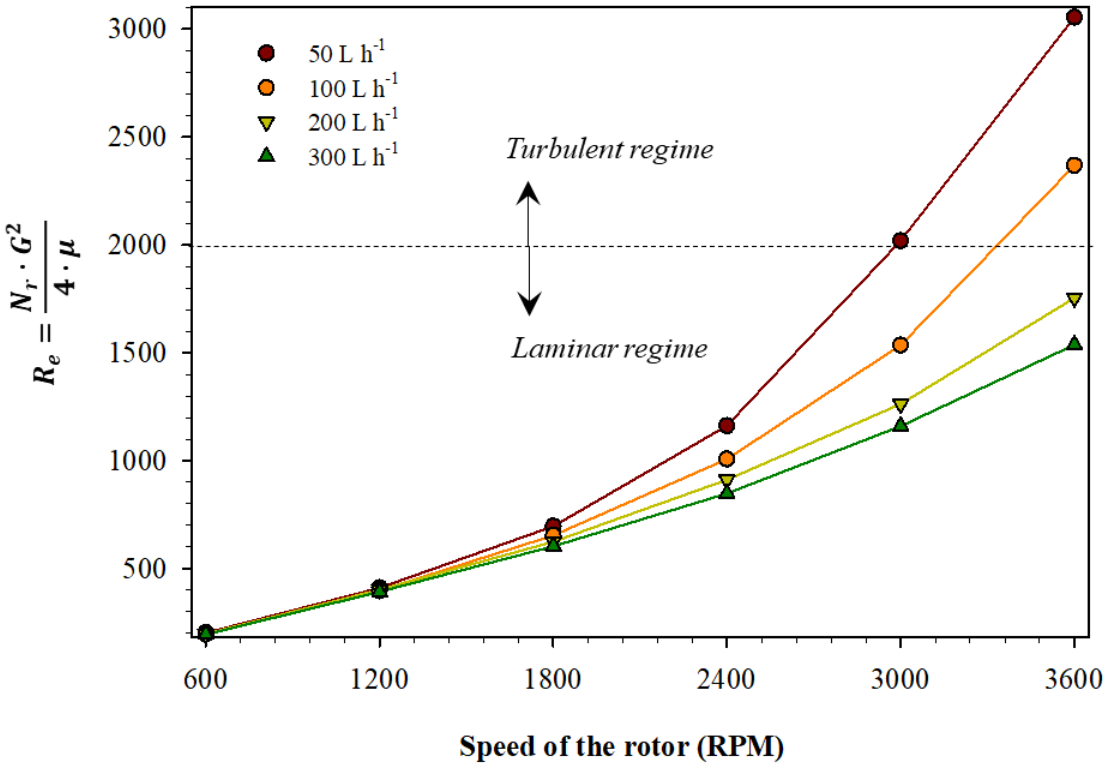

Figure 4. Effect of the speed of the rotor and volumetric flow rate on the Reynolds number.

Cavitation parameters

A common feature during the study of the flow in a rotor-stator device is the inter-relationship of the main operating variables (flow rate, pressure, and speed of the rotor). For instance, an increase in the upstream flow rate will result in an equal change of the inlet pressure, and an increase in the speed of the rotor equally change the outlet pressure. In an attempt to reduce the interrelationship of the operating variables, the pressure ratio ($r = {}^{p_1}/_{p_2}$) was selected for further analysis since it accounts for changes in the flow

rate, inlet pressure, speed of the rotor, and outlet pressure. Another relevant parameter for the analysis of the rotational cavitator is the pressure coefficient (C_p), a non-dimensional coefficient that expresses the pressure induce by the fluid at a specific position relative to the upstream or inlet pressure. C_p is only function of the geometry of the device for a given fluid. A graphical representation of these two dimensionless variables is given in **Figure 5**, where the pressure coefficient (C_p) is plotted as a function of the pressure ratio ($r = {p_1}/{p_2}$).

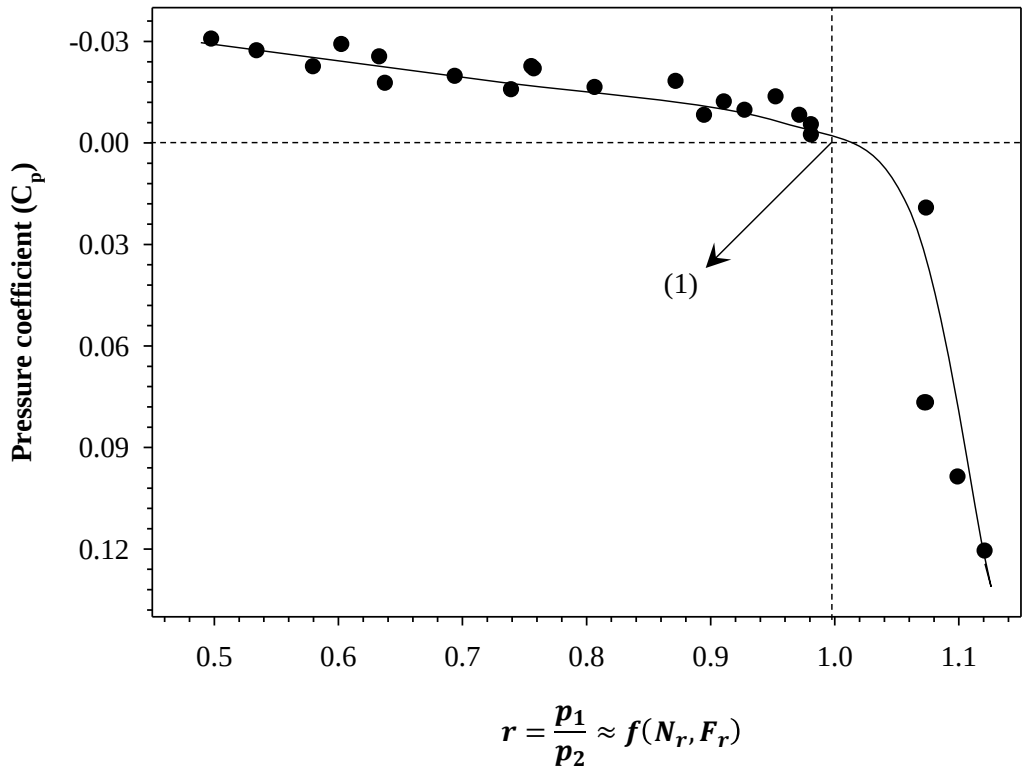

Figure 5. Effect of the pressure ratio ($r = {p_1}/{p_2}$) on the pressure coefficient Pressure coefficient (C_p).

The pressure ratio varied from 1.21 to 0.491 within the experimental domain. For simplicity, the pressure ratio has been divided into three regions corresponding to $r > 1$,

$r = 1$, and $r < 1$. The first scenario ($r > 1$) occurs when the outlet pressure is lower than the inlet pressure due to pressure losses within the cavitator, and it corresponds to the lower spectrum of the speed of the rotor, 600-1200 RPM. Values of pressure ratio equal to one take place when the inlet pressure and the outlet pressure are numerically equal. It is assumed that under such circumstances the phenomenon of cavitation has not yet developed. The final scenario ($r < 1$) occurs when the pressure generated due to the rotation is higher than the inlet pressure, and it results in the development of cavitation.

Figure 5 also shows the C_p varied from positive to negative values with decreasing the pressure ratio from 1.21 to 0.49. An interesting observation in the analysis of the C_p is the transition point from positive to negative (arrow (1) in **Figure 5**). Positive values of the C_p mean that the surface pressure which is generated by the rotor is higher than the static pressure (inlet pressure). The positive values of C_p were obtained within the range of pressure ratio of 1.21-1.00. Arrow (1) (**Figure 5**) corresponds to C_p of zero and $r = 1$, and it means the existence of the static point (generated pressure becomes equal to the inlet pressure). As the pressure ratio become lower than one, the C_p yielded negative values which indicates that the surface pressure generated by the rotor is much higher than the static or inlet pressure. For a given liquid flowing through a rotational cavitator, there will be a particular location at which the pressure is the minimum ($p_{min} \approx p_v$). Such relation is known as minimum pressure coefficient (C_{pmin}), and it expressed by Equation (7). The value of C_{pmin} helps to establish the minimum pressure needed at which the cavitation would first appear.

Figure 6 illustrates the different pressures involve in the analysis of the rotational cavitator: inlet pressure (p_1), outlet pressure (p_2), cavitation pressure (p_{app}), and vapor pressure (p_v). For illustration purpose, the y-axis is expressed in logarithmic scale. The inlet pressure was kept constant throughout the experiments (~104, 000 Pa), while the outlet pressure increased with the pressure ratio, which in turns depends on the speed of the rotor and the volumetric flow rate. The pressure at which cavitation would first appear also increased with the pressure ratio, suggesting that the appearance of the cavitation is only function of the velocity of the fluid for a given geometry, fluid density, and temperature.

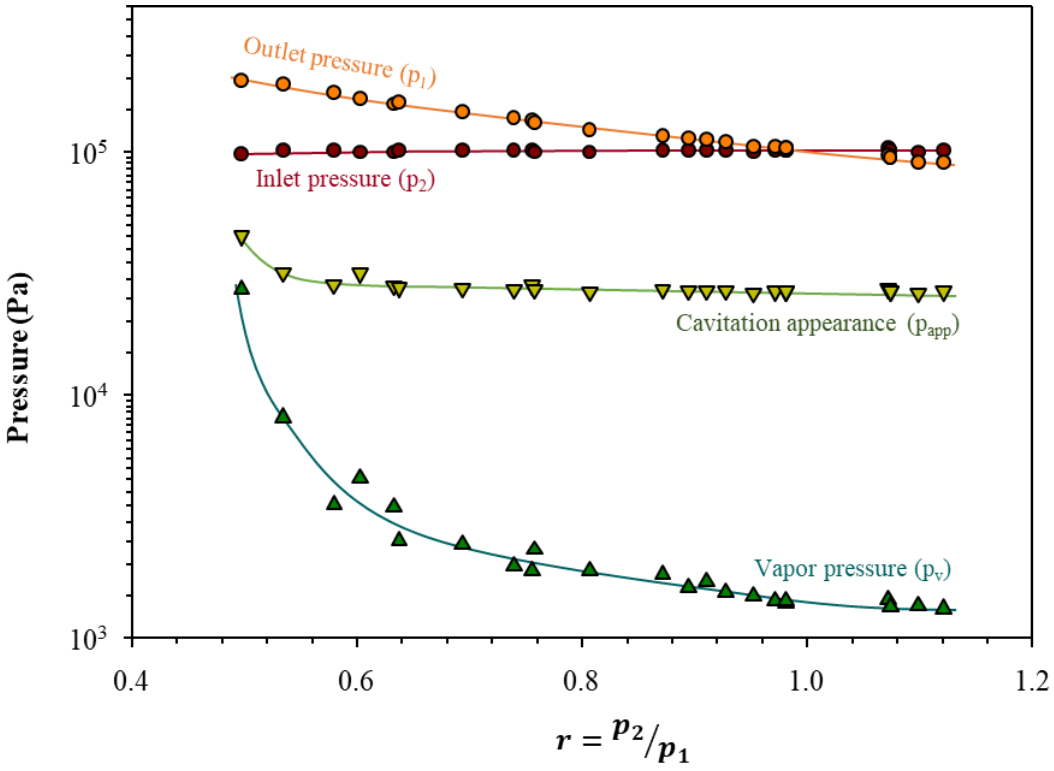

Figure 6. Distribution of pressures during the analysis of the rotational cavitation.

The development of the cavitation depends on a number of factors (flow rate, speed of the rotor, temperature, geometry of the device, and fluid properties), and it is commonly assumed that cavitation starts as soon as the pressure of the fluid falls below the vapor pressure. **Figure 7** shows the effect of the Reynolds number on the cavitation phenomenon. The development of the cavitation was predicted using the dimensionless number known as cavitation number, C_v. The cavitation number decreased exponentially from 1.15 to 0.04 with decreasing the pressure ratio. Similarly, Balasundaram & Harrison, (2006a) achieved maximum disruption of cells using a C_v of 0.125 within a hydrodynamic cavitation. An investigation on the optimization of the geometry for cell disruption by hydrodynamic cavitation showed an optimum C_v between 0.18 to 0.14 (Balasundaram & Harrison, 2011). Another investigation showed maximum disruption of brewers' yeast when the C_v was within the range of 0.17-0.09 (Balasundaram & Harrison, 2006b). Badve et al. (2013) used a rotational cavitator for reducing the organic load of wastewater, and it was found that a C_v of 0.40 effectively reduced the chemical oxygen demand. It is worth to mention that the development of cavitation and therefore its prediction depend on a number of factors (flow rate, geometry of the device, flow conditions, and others). Already, Šarc et al. (2017) pointed out that C_v cannot be used as single parameter for the evaluating of cavitation effect.

The C_v relates the collapsing forces of the cavities to the initial forces required to form the bubbles (Balasundaram & Harrison, 2006a). Values of C_v lower than one indicate that the inlet pressure (initial forces) is less than the velocity generated in the gap (collapsing forces), meaning that part of the excess energy is being utilized for the

generation of vapor pressure. Therefore, lower values of the C_v are indicative of more energy is utilized for the cavitation process (Badve et al., 2013). Overall, the cavitation takes place when the cavitation number lies below 1.0 (Gogate & Pandit, 2000). However, the presence of dissolved gases and suspended particles enhance the nucleation process and impact the development of the cavitation. Moreover, the flow conditions strongly influence the development of cavitation (**Figure 7**). The cavitation number decreases gradually with increasing the Reynolds number. A closer inspection of the Reynolds number (Equation (5)) reveals that an increase in the Reynolds number also involves a reduction in the kinematic viscosity of the fluid due to the elevation of the fluid temperature. A less viscous fluid results in higher Reynolds number which causes stronger cavitation (Mohan, Yang, & Chou, 2014).

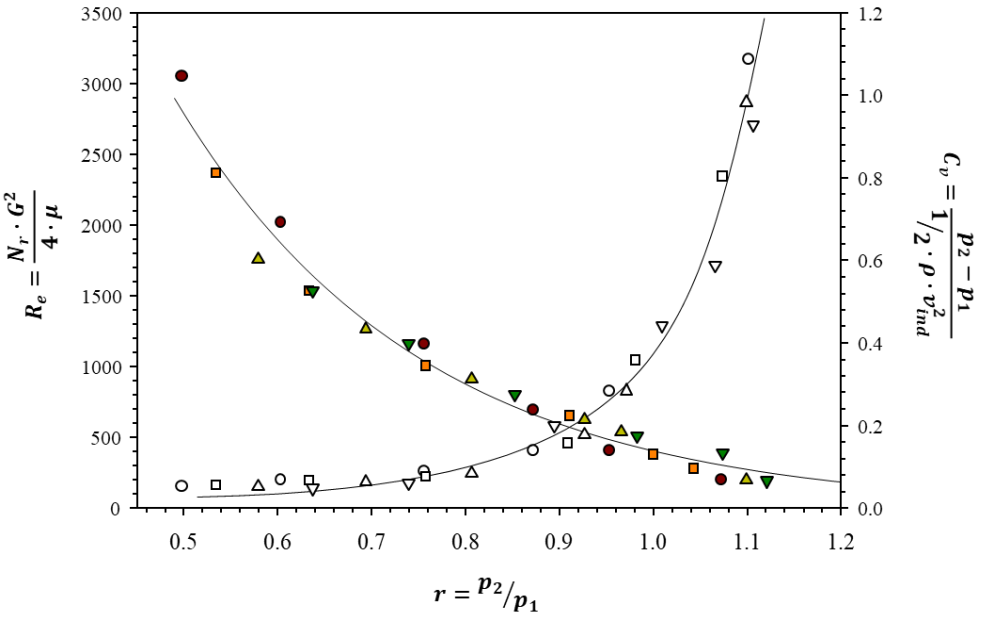

Figure 7. Effect of Reynolds number and pressure ratio on the cavitation number. ● – 50; ■ – 100; ▲ – 200; and ▼ – 300 L h^{-1}. Closed symbols correspond to Reynolds number; open symbols correspond to cavitation number.

The generated thermal energy due to cavitation as a function of the speed of the rotor is given **Figure 8**. The speed of the rotor expressed by RPM represents the physical constrains of the equipment, $0 \leq Speed \leq 3600\ RPM$. For instance, a value of zero of the speed of the rotor corresponds to no cavitation effect, while a speed of 3600 RPM indicates the maximum cavitation effect for a given flow rate. Overall, the thermal energy generated due to cavitation increased with the speed of the rotor in an exponential fashion, regardless of the flow rate.

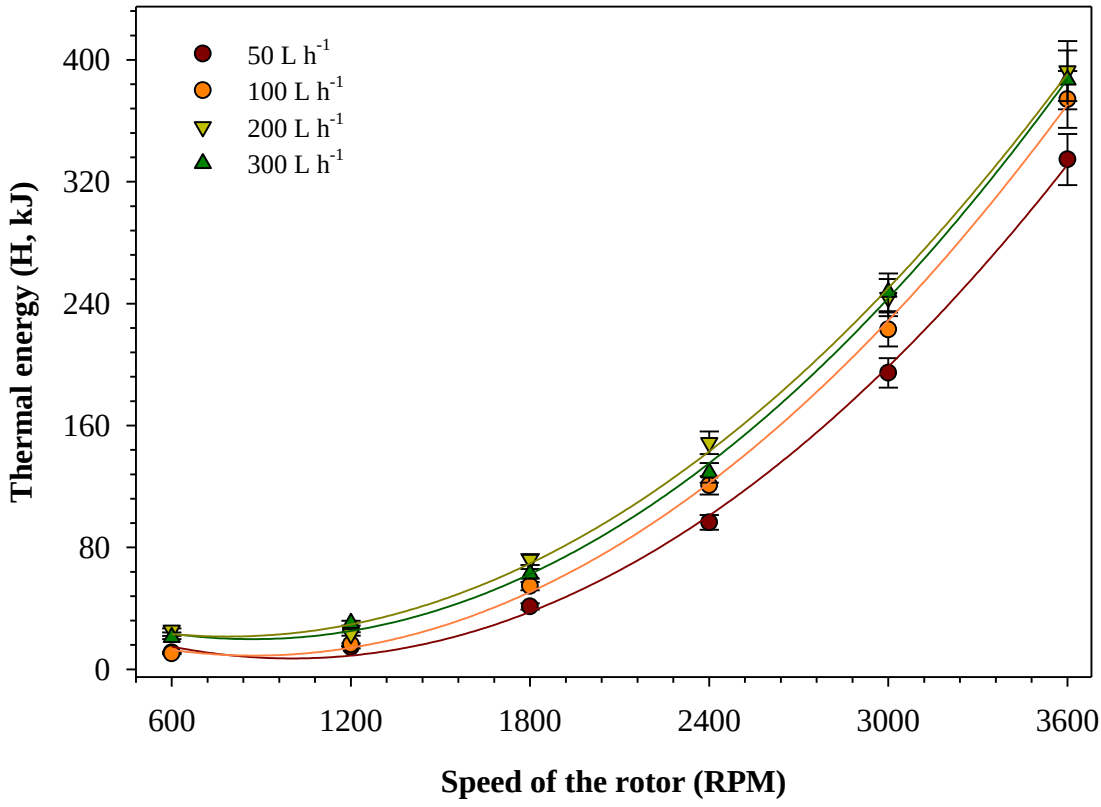

Figure 8. Thermal energy generated due to the rotational cavitator at different flow rates.

At the low spectrum of the rotor speed (600-1200 RPM), a relatively small amount of energy was generated, varying from 10 to 30 kJ without showing any particular pattern. Contrary, large amount of energy was generated as the speed of rotor increased (1800-

3600 RPM), reaching values up to 100-392 kJ. Kim et al. (2019) compared the thermal energy generated by a rotational device having an inner cylinder with and without indentations. These authors reported values of thermal energy between 29 and 126 kJ for the inner cylinder without indentations, and values of 326-803 kJ for the inner cylinder having indentations. The amount of energy generated in the absence of cavitation (inner cylinder without indentation) is negligible compared with that amount of thermal energy generated by rotational cavitation (cylinder with indentation). The energy released during the cavitation can be used as an indicator of the existence of cavitation. It is our assumption that the experimental measurement of ΔT_C is an indicator of the presence of hydrodynamic cavitation. Thus, below the critical value (<1800 RPM) the cavitation effect is minimal and the cavitator mainly serves as a mixing device. Contrary, samples treated above the critical frequency experience cavitation effect judging by the increase in the temperature. Further experiments were conducted within speed of the rotor range of 2400-3600 RPM.

Modeling the temperature increase due to cavitation

Figure 9 shows the increase in the fluid temperature due to hydrodynamic cavitation (ΔT_C) at different flow rates. Overall, the values of ΔT_C increased with the speed of the rotor, being more notorious at lower flow rates (>100 L h^{-1}). The highest ΔT_C was 57.6 ± 2.88 and 32.20 ± 1.61°C, followed by 16.90 ± 0.84 and 11.10 ± 0.55°C for 50, 100, 200, and 300 L h^{-1}, respectively. A closer inspection of the relationship between ΔT_C and speed of the rotor reveals the existence of a critical value below (arrow (1) in **Figure 9**) which the ΔT_C is negligible, and above which the ΔT_C becomes notorious. Hydrodynamic

cavitation involves the formation, growth, and collapse of vapor bubbles with the subsequent energy release in the form of shock waves (Badve et al., 2015). Most the release energy is adsorbed and redistributed within the liquid, while a small amount is lost through heat due to viscous forces. It is our assumption that the experimental measurement of ΔT_C is an indicator of the presence of hydrodynamic cavitation. Thus, below the critical value (<1800 RPM) the cavitation effect is minimal and the cavitator mainly serves as a mixing device. Contrary, samples treated above the critical frequency experience cavitation effect judging by the increase in the temperature. Further experiments were conducted within speed of the rotor range of 2400-3600 RPM.

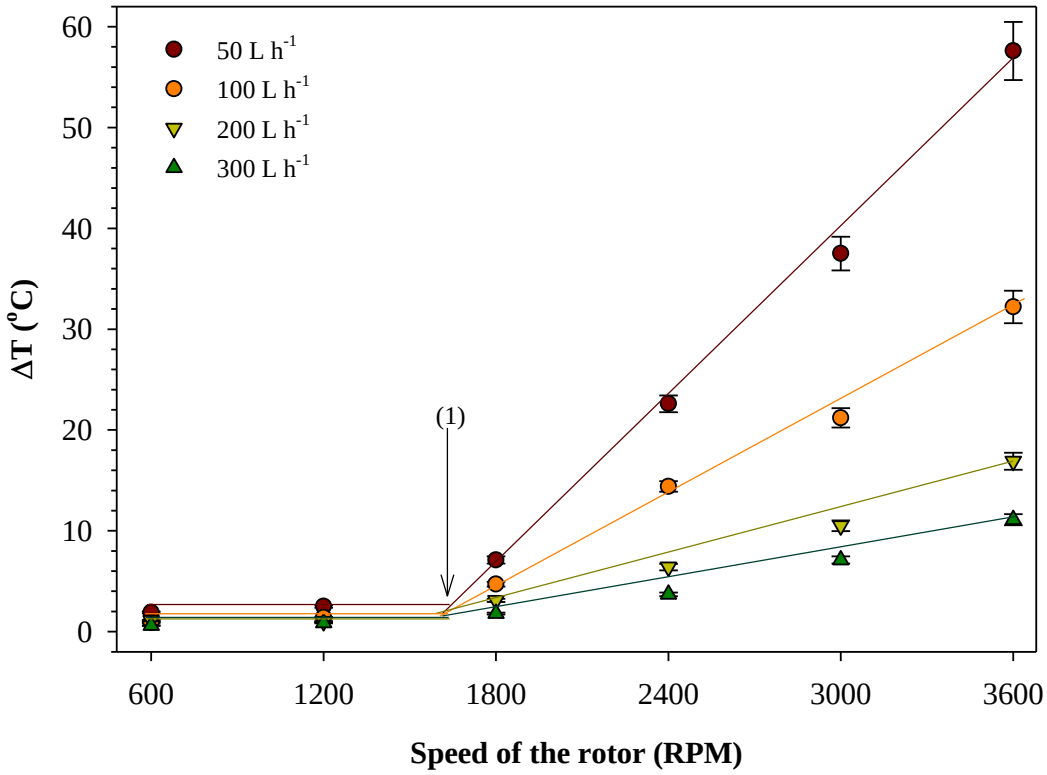

Figure 9. Temperature increase due to hydrodynamic cavitation as a function of speed of the rotor and flow rate.

The influence of total solids and flow rate on the ΔT_C is shown in **Figure 10**. Overall, the ΔT_C increased gradually with the total solids at a given flow rate and a speed of the rotor 3000-3600 RPM (**Figure 10a-b**). At 3600 RPM and 100 L h^{-1}, the ΔT_C increased from 33.32 ± 0.83 to 43.06 ± 0.73°C within the solids range of 0-36%. On the other hand, increasing the flow rate up to 300 L h^{-1} yields lower values of ΔT_C compared to that obtained at 100 and 200 L h^{-1}. Contrary, the ΔT_C slightly increased with the total solids regardless of the flow rate (**Figure 10c**). These observations have been exemplified by Badve et al. (2015) who performed finite element simulations of water flowing inside the cavitator. These authors found that high flow rates generate parabolic velocity profiles within the cavitator that may form cavity cloud, a phenomenon that diminish the collapse of cavities and hence lowering the ΔT_C. In an attempt to describe ΔT_C as a function of total solids, flow rate, and speed of the rotor, $\Delta T_C = f(TS, FR, Sp)$, experimental data were fitted to a second order polynomial equation (Equation (14)):

Equation (14)

$$\Delta T_C = a + b \cdot TS + c \cdot FR + d \cdot Sp + e \cdot TS * FR + f \cdot TS \cdot Sp + g \cdot FR \cdot Sp + h \cdot TS^2 + i \cdot FR^2 + j \cdot Sp^2$$

where *TS* is the total solids of the skim milk concentrate (%); *FR* is the flow rate through the cavitator (L h^{-1}); *a-e* are regression parameters with respect to *TS* and *FR*. The values of regression parameters and their fitting performance are shown in **Table 1**. The relation between predicted and experimental values of ΔT_C showed a relative narrow predicted and confidence band (**Figure 11**).

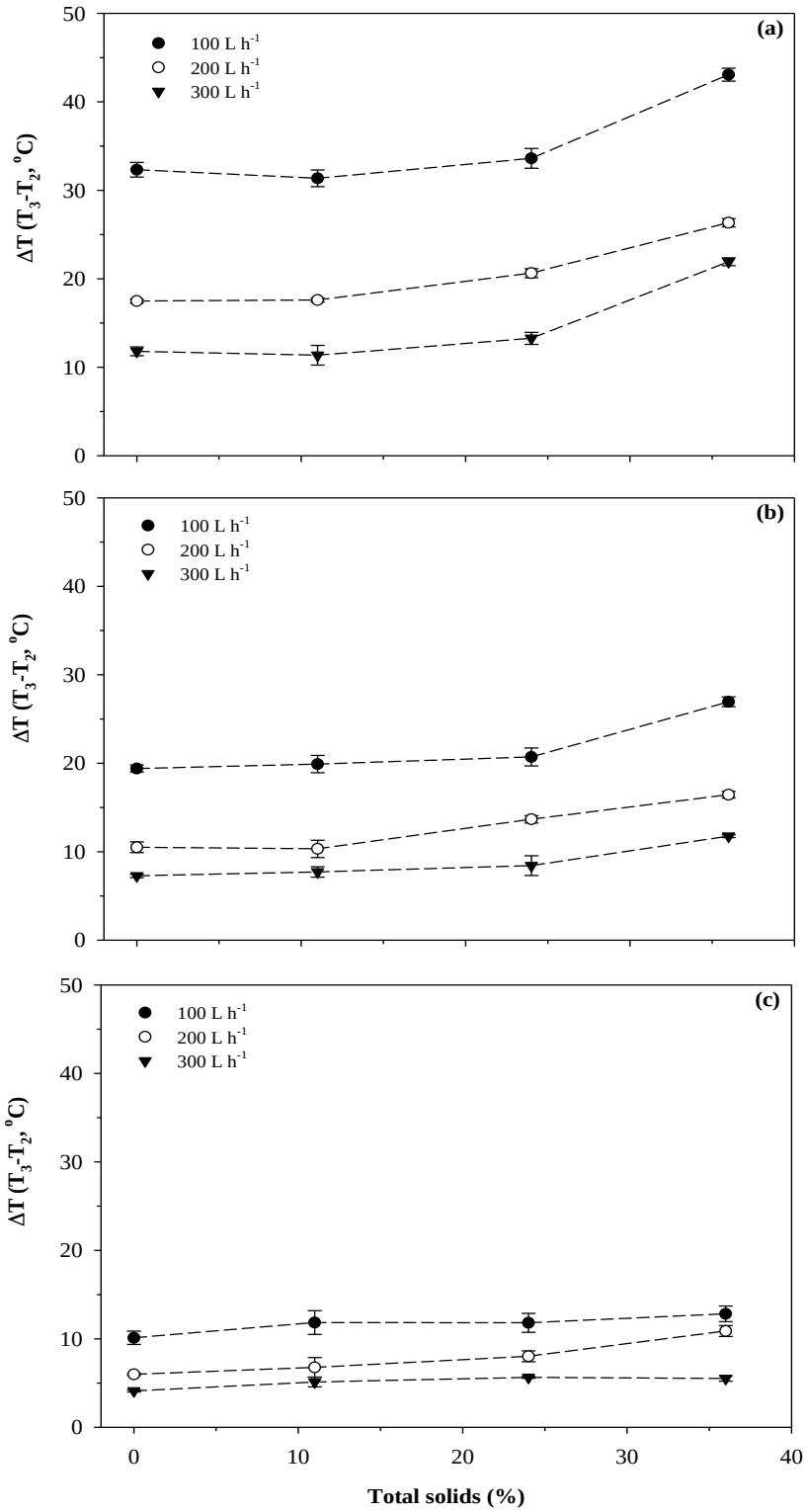

Figure 10. Influence of total solids and flow rate on the temperature increase due to hydrodynamic cavitation. Speed pf the rotor of (a) 3600, (b) 3000, (c) 2400 RPM, respectively. Initial product temperature 15 ± 1°C.

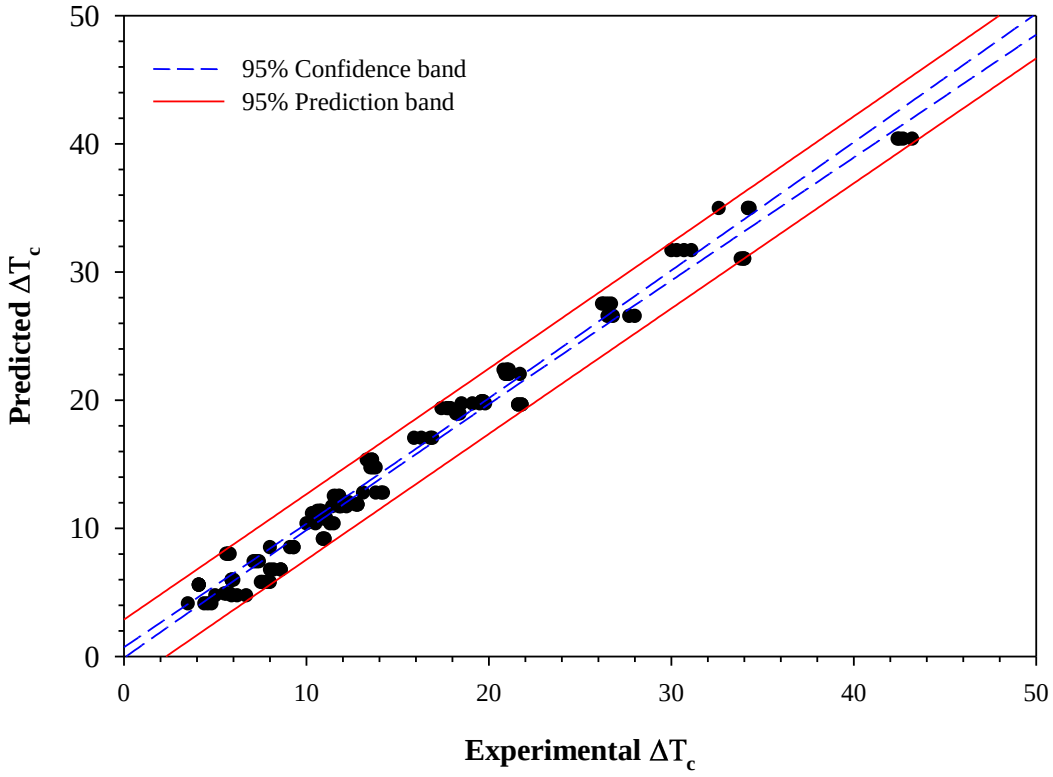

Figure 11. Linear relation between predicted and experimental ΔTC values. Continuous line represents 95% confidence band and discontinuous line represent 95% prediction band.

Table 1. Polynomial regression coefficients used to predict the temperature increase due to cavitation in skim milk concentrate. Parameters were obtained from Equation (14)

Parameter	Value ± CI95%
a	0.229 ± 0.011
b	-0.453 ± 0.044
c	$5.49\text{x}10^{-3} \pm 2.23\text{x}10^{-4}$
d	$2.71\text{x}10^{-4} \pm 9.31\text{x}10^{-6}$
e	$-2.18\text{x}10^{-4} \pm 2.41\text{x}10^{-5}$
f	$1.24\text{x}10^{-4} \pm 1.14\text{x}10^{-5}$
g	$-5.59\text{x}10^{-5} \pm 6.71\text{x}10^{-6}$
h	$7.99\text{x}10^{-3} \pm 7.83\text{x}10^{-4}$
i	$2.51\text{x}10^{-4} \pm 2.47\text{x}10^{-5}$
j	$3.62\text{x}10^{-6} \pm 3.21\text{x}10^{-7}$
R^2	0.981
R^2_{adj}	0.979

CI95% — 95% confidence interval; R^2 — coefficient of determination; R^2_{adj} – adjusted coefficient of determination

2.4. Conclusions

The analysis of the cavitator reveals that the velocities generated inside the rotational cavitator are sufficiently high to induce cavitation within the fluid. The development of the cavitation was influenced by the flow rate, speed of the rotor, temperature, and fluid properties. The pressure at which cavitation would first appear was calculated as a function of the operating parameters. Moreover, the distribution of pressure within the cavitator was established as a function of operating parameters. The analysis of the cavitation parameters showed the existence of a threshold rotation speed (1200 RPM), exhibiting a significant correlation between fluid velocity, increase in the fluid temperature, and cavitation number. The increase in the temperature of the fluid was modeled, showing satisfactory correlation with the experimental data.

2.5. References

Ahmed, S. M. (1998). Investigation of the temperature effects on induced impact pressure and cavitation erosion. Wear, 218(1):119-127.

Arrojo, S., & Benito, Y. (2008). A theoretical study of hydrodynamic cavitation. Ultrasonics Sonochemistry, 15(3):203-211.

Badve, M., Gogate, P., Pandit, A., & Csoka, L. (2013). Hydrodynamic cavitation as a novel approach for wastewater treatment in wood finishing industry. Separation and purification technology, 106, 15-21.

Badve, M. P., Bhagat, M. N., & Pandit, A. B. (2015). Microbial disinfection of seawater using hydrodynamic cavitation. Separation and purification Technology, 151:31-38.

Badve, M. P., Alpar, T., Pandit, A. B., Gogate, P. R., & Csoka, L. (2015). Modeling the shear rate and pressure drop in a hydrodynamic cavitation reactor with experimental validation based on KI decomposition studies. Ultrasonics & Sonochemistry, 22: 272-277.

Balasundaram, B., & Harrison, S. T. L. (2006a). Study of physical and biological factors involved in the disruption of *E. coli* by hydrodynamic cavitation. Biotechnology progress, 22(3):907-913.

Balasundaram, B., & Harrison, S. T. L. (2006b). Disruption of Brewers' yeast by hydrodynamic cavitation: process variables and their influence on selective release. Biotechnology and bioengineering, 94(2):303-311.

Balasundaram, B., & Harrison, S. T. L. (2011). Optimising orifice geometry for selective release of periplasmic products during cell disruption by hydrodynamic cavitation. Biochemical engineering journal, 54(3):207-209.

Carlton, J. S. (2012). Cavitation. In J. S. Carlton (Ed.), *Marine propellers and propulsion*: Butterworth-Heinemann, Oxford.

Chahine, G. L. (1997). Numerical simulation of cavitation dynamics. Paper presented at the Proceedings of the 2nd LAAS Conference on Computer Simulation, Beirut, Lebanon.

Endo, H. (1994). Thermodynamic consideration of the cavitation mechanism in homogeneous liquids. The Journal of the Acoustical Society of America, 95(5):2409-2415.

Griggs, J. L. (2015). Apparatus for heating fluids. US 20150176836A1.

Gogate, P. R., & Pandit, A. B. (2000). Engineering design methods for cavitation reactors II: hydrodynamic cavitation. AIChE journal, 46(8):1641-1649.

Gogate, P. R., & Pandit, A. B. (2005). A review and assessment of hydrodynamic cavitation as a technology for the future. Ultrasonics sonochemistry, 12(1-2):21-27.

Gregersen, S. B., Wiking, L., Bertelsen, K. B., Tangsanthatkun, J., Pedersen, B., Poulsen, K. R., Andersen, U., & Hammershøj, M. (2019). Viscosity reduction in concentrated protein solutions by hydrodynamic cavitation. International Dairy Journal, 97:1-4.

Habashi, N., Mehrdadi, N., Mennerich, A., Alighardashi, A., & Torabian, A. (2016). Hydrodynamic cavitation as a novel approach for pretreatment of oily wastewater for anaerobic co-digestion with waste activated sludge. Ultrasonics sonochemistry, 31:362-370.

Innings, F., Hultman, E., Forsberg, F., & Prakash, B. (2011). Understanding and analysis of wear in homogenizers for processing liquid food. *Wear, 271*(9):2588-2598.

Jian, W., Petkovšek, M., Houlin, L., Širok, B., & Dular, M. (2015). Combined numerical and experimental investigation of the cavitation erosion process. Journal of Fluids Engineering, 137(5):051302.

Kim, H., Koo, B., Lee, S., & Yoon, J. Y. (2019). Experimental study of cavitation intensity using a novel hydrodynamic cavitation reactor. Journal of Mechanical Science and Technology, 33(9):4303-4310.

Kumar, P. S., & Pandit, A. B. (1999). Modeling hydrodynamic cavitation. Chemical Engineering & Technology: Industrial Chemistry-Plant Equipment-Process Engineering-Biotechnology, 22(12):1017-1027.

League, R. D., & Parker, D. E. (2009). Controlled cavitation device with easy disassembly and cleaning. US 007507014B1.

Li, K., Woo, M. W., Patel, H., Metzger, L., & Selomulya, C. (2018). Improvement of rheological and functional properties of milk protein concentrate by hydrodynamic cavitation. Journal of Food Engineering, 221:106-113.

Li, C., Yang, F., Huang, Y., Huang, C., Zhang, K., & Yan, L. (2020). Comparison of hydrodynamic and ultrasonic cavitation effects on soy protein isolate functionality. Journal of Food Engineering, 265:109697.

Mancuso, G., Langone, M., & Andreottola, G. (2017). A swirling jet-induced cavitation to increase activated sludge solubilisation and aerobic sludge biodegradability. Ultrasonics sonochemistry, 35:489-501.

Mohan, B., Yang, W., & Chou, S. (2014). Cavitation in injector nozzle holes–a parametric study. Engineering Applications of Computational Fluid Mechanics, 8(1):70-81.

Patil, P. N., Gogate, P. R., Csoka, L., Dregelyi-Kiss, A., & Horvath, M. (2016). Intensification of biogas production using pretreatment based on hydrodynamic cavitation. Ultrasonics sonochemistry, 30:79-86.

Petkovšek, M., Zupanc, M., Dular, M., Kosjek, T., Heath, E., Kompare, B., & Širok, B. (2013). Rotation generator of hydrodynamic cavitation for water treatment. Separation and Purification Technology, 118:415-423.

Petkovšek, M., & Dular, M. (2013). Simultaneous observation of cavitation structures and cavitation erosion. Wear, 300(1-2):55-64.

Petkovšek, M., & Dular, M. (2017). Observing the thermodynamic effects in cavitating flow by IR thermography. Experimental Thermal and Fluid Science, 88:450-460.

Šarc, A., Stepišnik-Perdih, T., Petkovšek, M., & Dular, M. (2017). The issue of cavitation number value in studies of water treatment by hydrodynamic cavitation. Ultrasonics sonochemistry, 34:51-59.

Šarc, A., Stepišnik-Perdih, T., Petkovšek, M., & Dular, M. (2017). The issue of cavitation number value in studies of water treatment by hydrodynamic cavitation. Ultrasonics sonochemistry, 34:51-59.

Šarc, A., Kosel, J., Stopar, D., Oder, M., & Dular, M. (2018). Removal of bacteria Legionella pneumophila, Escherichia coli, and Bacillus subtilis by (super) cavitation. Ultrasonics Sonochemistry, 42:228-236.

Sano, Y., & Usui, H. (1985). Interrelations among mixing time, power number and discharge flow rate number in baffled mixing vessels. Journal of chemical engineering of Japan, 18(1):47-52.

Stoop, A.H., Bakker, T.W., & Kramer, H.J.M., (2015). Cavitation for improved sludge conversion into biogas. Journal of Physics: Conference Series. 656:12118.

van Wijngaarden, L. (2016). Mechanics of collapsing cavitation bubbles. Ultrasonics Sonochemistry, 29:524-527.

Chapter 3

Application of Hydrodynamic Cavitation in Skim milk Concentrate: Process Characterization and Microbial Efficiency

3.1. Introduction

The global market of whole milk and skimmed milk powder has increased from about $27 million U.S. dollar in 2017 to over $30 million U.S. dollar in 2019, and it is projected to exceed $38 million by 2025 (Anonymous 2019). The manufacture of such powders involves a number of unit operations including separation, thermal treatment, evaporation, and drying. Specific details on the manufacture of milk powder can be found elsewhere (Walstra, Wouters, & Geurts, 2006).

A key processing step during the manufacture of skimmed milk powder is the thermal treatment, where the combinations of temperature and time determine the functional properties of the powder. The intensity of the thermal treatment measured by the Whey Protein Nitrogen Index (WPNI) is used to classify the skimmed milk powders as low-heat (WPNI ≥6.0), medium-heat (WPNI 4.5-5.9), and high-heat powder (WPNI ≤1.5) (Sharma, Jana, & Chavan, 2012). **Table 2** summarizes the classification of milk powders based on heat treatments. A powder classified as low-heat is typically obtained by a thermal treatment of 70°C for 15 s before evaporation. Low-heat powder is the most soluble form of milk powder, and it is used extensively in formulating bakery, confectionary, ice-cream, and infant formula.

Table 2. Classification of milk powder based on the applied thermal treatment. Adapted from Sharma, Jana, & Chavan, (2012).

Powder classification	Processing conditions	Whey Protein Nitrogen Index	Functional properties
Low-heat	70°C/15 s	≥6.0	- Highly soluble
Medium-heat	85°C/60 s	4.51-5.99	- Emulsification
High-heat	120°C/120 min	≤1.50	- Heat stability, gelation

Whey protein nitrogen index (mg undenatured protein per gram of powder)

During the manufacture of low-heat powder, the thermal treatment is the highest temperature applied, and it is aimed at ensuring the microbiological quality of the final powder. However, thermoduric organisms are capable of surviving such thermal treatment (75°C for 15 s), and they can sporulate downstream. This has been exemplified by Reich et al. (2017), who identified thirteen thermophilic bacilli as the major contaminants of milk powders. More importantly, it was emphasized that High-Temperature-Short-Time (HTST) pasteurization is not sufficient for producing low-spore powder. The presence of thermoduric bacteria in milk powders is an indication of poor hygienic protocols within the manufacturing plant (Burgess, Lindsay, & Flint, 2010). Moreover, thermoduric bacteria can produce proteolytic enzymes that results in the formation of off-flavor compounds.

The rate at which the thermoduric bacteria sporulate has been investigated by Scott et al. (2007), who identified two main points of cell growth and sporulation during the manufacture of milk powders, namely the preheating sections and during the evaporation.

The temperature of these points typically varies between 45 to 75°C, which corresponds to the ideal temperature growth of thermophilic organisms. Indeed, Ali et al. (2013) reported between 2.1 and 4.8 log CFU g^{-1} of heat-resistant bacteria in commercial samples of skim milk powder. Similarly, Buehner, Anand, & Djira, (2015) reported 3.5 log CFU g^{-1} of thermoduric bacteria in commercial samples of skim milk powder.

Sterilization treatments such as Ultra-High-Temperature (UHT) pasteurization (130-145°C for > 4s) and canning in retort (120°C for 30 min) destroy residual spoilage microorganisms and their spores. However, the principal limitation of UHT is the relatively slow mode of heat transfer (convection and conduction) during heating and holding, which often leads to many unintended adverse effects such as nutrient destruction, protein denaturation, and formation of toxins and off-flavor compounds (Hill & Smythe, 2012). Thus, the application of UHT results in the denaturation of whey proteins, and the resulting product cannot be classified as low-heat powder. Alternatively, the use of emerging technologies has gained a great deal of attention due to their ability to reduce the microbial load with reduced thermal damage. UV-irradiation, thermo-sonification, and ultrasound are examples of such technologies aimed at producing low-spore milk powders. Ansari, Ismail, & Farid, (2017) reduced 2 log CFU g^{-1} of *Bacilus Subtilis* spores in whole milk using an ultrasound treatment (1.1 W mL^{-1}) combined with thermal energy, 100°C. Khanal et al. (2014) used skim and whole milk to study the effect of high intensity ultrasound combined with thermal energy on the inactivation of vegetative cells of spore forming *Bacillus* spp. These authors reported an inactivation of 4.5 logs of *B. coagulans* by the application of ultrasound (80% amplitude for 10 min). In

summary, the inactivation of spore formers by means of ultrasound involves prolonged exposure time (> 5 min), which limits the applicability of ultrasound at industrial level.

Another technological option recently explored is the thermal treatment of the concentrated milk between or after the evaporation (Wedel et al., 2018). Such approach is not a trivial task since aggregation of proteins may occur at high total solids, resulting in coagulation of the concentrated milk (Dumpler & Kulozik, 2016). Moreover, the published information regarding the thermal inactivation of thermoduric bacteria involved the glass capillary method, a procedure where the heat transfer limitations are neglected. In the case of concentrated milk; however, the thermal transfer within the liquid is not homogenous due to the induced aggregation and increased viscosity. Research on the inactivation of thermoduric bacteria in concentrated milk is scarce, and badly needed. A promising technology under development at South Dakota State University consists in combining the energy released by a rotational cavitator with thermal treatment to reduce the levels of thermoduric sporeformers. Therefore, the objective of this chapter is to develop an experimental rig for the reduction of thermoduric sporeformers in skim milk concentrate (SMC) by combining hydrodynamic cavitation and thermal treatment.

3.2. Materials and methods

Process diagram

The experiments were conducted using a pilot scale APV cavitator (SPX Flow Technology, Crawly West Sussex, United Kingdom) coupled with a custom fabricated

thermal treatment (**Figure 12**). The system consists of a feed tank, positive displacement pump, APV cavitator, plate heat exchanger, holding tube, and cooling system. A holding tube section with adjustable lengths was locally fabricated and it is capable of operating at different combinations of flow rate (100-600 L h-1) and holding time (6-70 s). The holding tube section was experimentally validated using the salt conductivity method. The holding tube assembly consisted of three sections of 0.9 m made of stainless steel connected by six elbows of 180°. An inclination of ¼ inch per ft was provided, as specified by FDA regulations. The experimental rig combined hydrodynamic cavitation coupled with thermal processing. The sample temperature in different processing steps (feed tank, after cavitation, before and after holding tube, and cooling) were monitored during experiments using K-type thermocouples connected to a data logger (Omega Engineering Inc., Stamford, CT). Heat losses within the holding tube were minimized by insulated using plumbing foam. The flow rate was measured using a flow meter (GPI A1, Instrumart Inc., South Burlington, VT).

Skim milk concentrate (SMC)

The microbial efficiency of the hydrodynamic cavitation was evaluated in reconstituted skim milk concentrate (34-36% total solids). Nonfat dry milk was dissolved in deionized for 30 min at 50-60°C under constant agitation. The reconstituted skim milk concentrate was cooled at room temperature and the total solids was measured with a diffractometer. Samples were stored overnight before the microbial analysis.

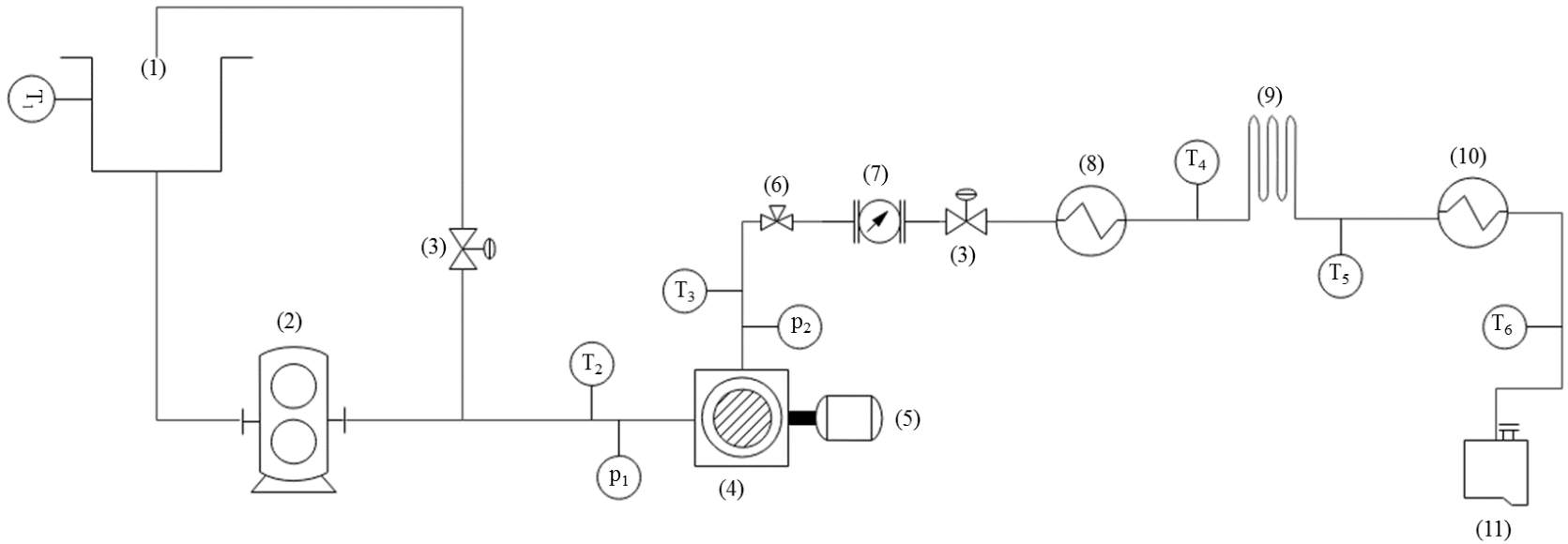

Figure 12. Flow diagram of the experimental apparatus: T_1 – temperature of untreated product; T_2 – product inlet temperature prior to cavitation; T_3 – temperature rise due to cavitation; T_4 – product temperature after heat exchanger; T_5 – product temperature after holding tube; and T_6 - product temperature after cooling heat exchanger; p_1 and p_2 – inlet and outlet pressure, respectively. (1) Feeding tank; (2) positive displacement pump; (3) flow regulator valve; (4) hydrodynamic cavitator; (5) hydraulic rotor; (6) sampling port; (7) flow meter; (8) plate heat exchanger; (9) holding tube; (10) cooling system; (11) semi-aseptic tank.

Preparation of Bacillus coagulans

A suspension of vegetative cells of *Bacillus coagulans* (ATCC 12245) was prepared as described by Khanal et al. (2014). Briefly, *B. coagulans* was grown in Brain Heart Infusion (Difco, Becton, Dickinson and Company, Sparks, NV, USA) for 8 h at 37°C under aerobic conditions. After the incubation, the solution was centrifuged at 4500 x g for 30 min using a Avanti JE centrifuge (Beckman Coutler Inc., CA, USA). The precipate was re-suspended in phosphate buffer saline (pH 7.4), and transferred into cryogenic vials. The vials were stored at -75°C using an ultralow deep freezer (NuAire Inc., Plymouth, MN, USA) until further use.

Inoculation and treatments

Ten liters of reconstituted skim milk concentrate were inoculated by adding 10 mL of the suspension of vegative cells of *B. coagulans*, yielding an approximate final concentration of 4.5 log CFU mL^{-1}. Nine time-temperature combinations were used to evaluate the microbial efficiency of the hydrodynamic cavitation coupled with thermal treatment in skim milk concentrate (75°C/15 s, 75°C/76 s, 75°C/106 s, 80°C/14 s, 80°C/26 s, 80°C/48 s, 85°C/14 s, 85°C/26 s, and 85°C/48 s) using a fixed flow rate of 100 L h^{-1} and a cavitation frequency of 3600 RPM. The selected processing conditions correspond to typical conditions used during the manufacture of skim milk powder. Before pumping the inoculated skim milk concentrate, the whole unit was run with a carboxymethylcellulose solution of the same apparent viscosity than the skim milk concentrate. The solution flowed until the desired flow rate and temperature were reached. Then, 10 L of skim milk concentrate ware introduced and the first 1 L of treated

product was discarded. Afterward, the samples of 500 mL were collected in pre-sterilized polypropylene tubes (Fisher, Rochester, USA). Three different treatments were performed to evaluate the microbial efficiency of the experimental rig, 1) hydrodynamic cavitation, 2) hydrodynamic cavitation followed by thermal treatment, and 3) thermal treatment. For the cavitation treatment, samples were obtained from the sampling port valve ((6) in **Figure 12**) located after the cavitator. Samples obtained at the end of the process ((11) in **Figure 12**) were considered for the hydrodynamic cavitation followed thermal treatment. In the case of the thermal treatment, samples were obtained at the end of the process with bypass the cavitator.

Enumeration of microorganisms

The viable cells of *B. coagulans* after treatments were enumerated on brain heart infusion agar. Series of dilutions were prepared by using phosphate buffer saline solution and plate with tryptic soy agar (0.015% tryptone, 0.005% soy tone, 0.0055 % sodium chloride, 0.015% agar, pH 7.3 ± 0.2). All plates were incubated at 37°C for 48 hours to enumerate total viable cells. After incubation, total colony forming units were enumerated according to Equation (15).

Equation (15)

$$N(CFU\ mL^{-1}) = \sum \frac{C}{\{(n_1 \times 1) + (n_2 \times 0.1)\} \cdot d}$$

Where, N is number of colonies per mL or g of product, $\sum C$ is Sum of all colonies on all plates counted, n_1 is number of plates in next higher dilution counted, n_2 is number of

plates in next higher dilution counted and d is dilution from which the first counts were obtained.

Decimal reduction time (D-values)

The thermal death time concept was used to calculate the decimal reduction time for of the *B. coagulans* (ACCT 12245) in skim milk concentrate. The decimal reduction time (D-values) is the time needed for a 90% reduction (1 log cycle), and it assumes that a first-order kinetic model describes the inactivation of the given microorganism. Thus, the kinetic model for the inactivation of *B. coagulans* follows a first-order behavior according to Equation (16).

Equation (16)

$$\ln N_t = \ln N_o - k \cdot t$$

Where N_t is the number of microorganism at a given time, N_o is the initial number of microorganisms, k is the first-order rate constant (s^{-1}), and t is the holding time (s). Equation (16) was further rearranged into:

Equation (17)

$$log\left(\frac{N_t}{N_o}\right) = \log S(t) - t \cdot D$$

where D is the decimal reduction time ($D = \frac{2.303}{k}$) and it is a reciprocal first-order rate constant. The D values at three different temperatures (75, 80, and 85°C) were obtained from the semi-logarithmic curve ($\log S(t)$ vs time) by non-linear regression analysis. Solver option in Excel Microsoft was used to perform the non-linear regression analysis, and the graphs were plotted using Sigmaplot software V11 for Windows (SPSS Inc., Chicago, IL, USA).

Statistical analysis

The statistical analysis was performed by the one-way analysis of the variance (ANOVA), and the least significant difference (LSD), in which a significant level was set at 0.05. The LSD values were calculated using Tukey's post hoc test, and all calculations were performed using the Statistical Package for R programing.

3.3. Results and discussion

Temperature history

Figure 13 shows a representative temperature history of SMC as it flows through the different component of the experimental rig (**Figure 12**). Two different process are illustrated: i) a typical HTST, and ii) a cavitation assisted HTST. In both cases, the process starts in the feeding tank where the temperature of the SMC varied from 10 to 12°C. The SMC flows through the rotational cavitator, where the temperature increased from 10-12 to 52-53°C due to energy released by the cavitation phenomenon.

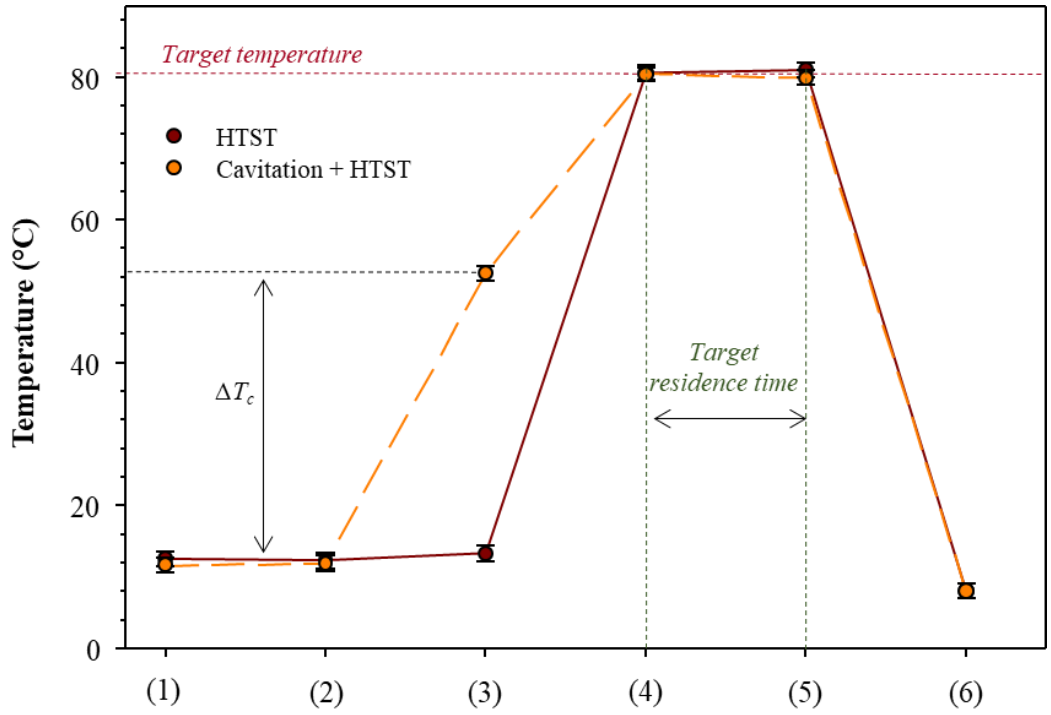

Figure 13. Representative temperature history of skim milk concentrate flowing through the different component of the experimental rig. The temperature values correspond to skim milk concentrate (34-36% total solids) flowing at 100 L h^{-1}, and cavitated at 3600 RPM. (1) temperature at the feeding tank; (2) inlet temperature of the cavitator; (3) outlet temperature of the cavitator; (4) temperature at the beginning of the holding tube; (5) temperature at the end of the holding tube; and (6) temperature after cooling.

The magnitude of such increment depends on the speed of the rotor and flow rate. Subsequently, the SMC is further heated at the target temperature (70-85°C) using a plate heat exchanger before entering the holding tube. The holding tube consists of different sections that can be adjusted to provide three different residence times (14-106 s) at a constant flow rate (100 L h^{-1}). The residence time was calculated using the salt test. Importantly, the temperature of the SMC remains unchanged between the beginning and end of the holding tube, regardless of the length. Knowledge of the residence time of the fasted moving particle in the holding tube is a critical parameter for further validation since the Food and Drug Administration (FDA) only credits heat treatment experienced

in the holding tube. After the corresponding residence time, the SMC is cooled down to <10°C using a tubular heat exchanger. Interestingly, the experimental rig can be manipulated to generate processing conditions similar to those obtained by conventional thermal treatment (70-85°C with residence time of 14-106 s) by suitable choice of initial temperature, speed of rotor, and flow rate. A detailed explanation of the temperature history within the experimental rig not only facilities the interpretation of the experimental findings but also stablish the foundations for further scaling-up.

Effect of residence time on the inactivation of B. coagulans

The thermal resistance of *B.coagulans* (ACCT 12245) in SMC was monitored at different points within the experimental rig, including after inoculation (feeding tank), after cavitation (3600 RPM at 100 L h^{-1}), after HTST (75-85°C for 14-106 s), and after hydrodynamic cavitation followed by HTST. **Figure 14** shows the log counts at different points within the experimental rig as well as the effect of residence time on the survivors of *B.coagulans*. For all treatments, the survivors of *B.coagulans* after cavitation were not significantly different in comparison with the inoculated sample (4.39 ± 0.41 and 4.75 ± 0.16 log CFU mL^{-1}). This observation is in agreement with the results reported elsewhere (Bawa, 2016), where significant reduction of *Bacillus coagulans* was observed after multiple passes in the rotational cavitator.

For HTST at 75°C (**Figure 14a**), a gradual reduction of the survivors was observed as the residence time was prolonged, reaching values of 2.1 ± 0.01, 1.68 ± 0.11, and 1.32 ± 0.01 log CFU mL^{-1} after 48, 76, and 106 s, respectively. Similar trend was observed in

the survivors after cavitation+HTST, where the final counts were 1.90 ± 0.01, 1.31 ± 0.11, and 1.10 ± 0.01 log CFU mL^{-1} after 48, 76, and 106 s, respectively. At 80°C (**Figure 14b**), the survivors decreased with the residence time, obtaining survivors values of 2.60 ± 0.05, 1.58 ± 0.15, 1.46 ± 0.11 log CFU mL^{-1} after 14, 26, and 48 s, respectively. The survivors when cavitation was followed by HTST at 80°C were 2.50 ± 0.13, 1.46 ± 0.07, 1.44 ± 0.11 log CFU mL^{-1} after 14, 26, and 48 s, respectively. In the case of 85°C (**Figure 14c**), the obtained survivors were 3.36 ± 0.03, 2.77 ± 0.03, 2.54 ± 0.02, and 2.03 ± 0.04 log CFU mL^{-1} after 14, 26, 38, and 48 s, respectively. Similar trend was observed in the survivors after cavitation+HTST, where the final counts were 2.82 ± 0.07, 2.36 ± 0.01, 2.06 ± 0.01, 1.81 ± 0.03 log CFU mL^{-1} after 14, 26, 38, and 48 s, respectively.

A 3.65 log reduction was obtained by cavitation-thermal treatment (75°C), while HTST along yielded a 3.06 log reduction. Contrary, the reduction values at 80°C were 3.01 and 3.42 log for HTST and cavitation followed by HTST, respectively. Finally, the reduction at 85°C was 2.10 and 2.34 log for HTST and cavitation followed by HTST, respectively. At 75°C, the combined effect of hydrodynamic cavitation and thermal treatment on the reduction of *B.coagulans* in skim milk concentrate is thought to be synergistic. However, this interpretation must be applied cautiously because the reduction of *B.coagulans* is affected by the initial counts of the powder used to formulate the milk concentrate (discontinuous line in **Figure 14**), and the resulting log reduction might not represent the actual lethality of the process.

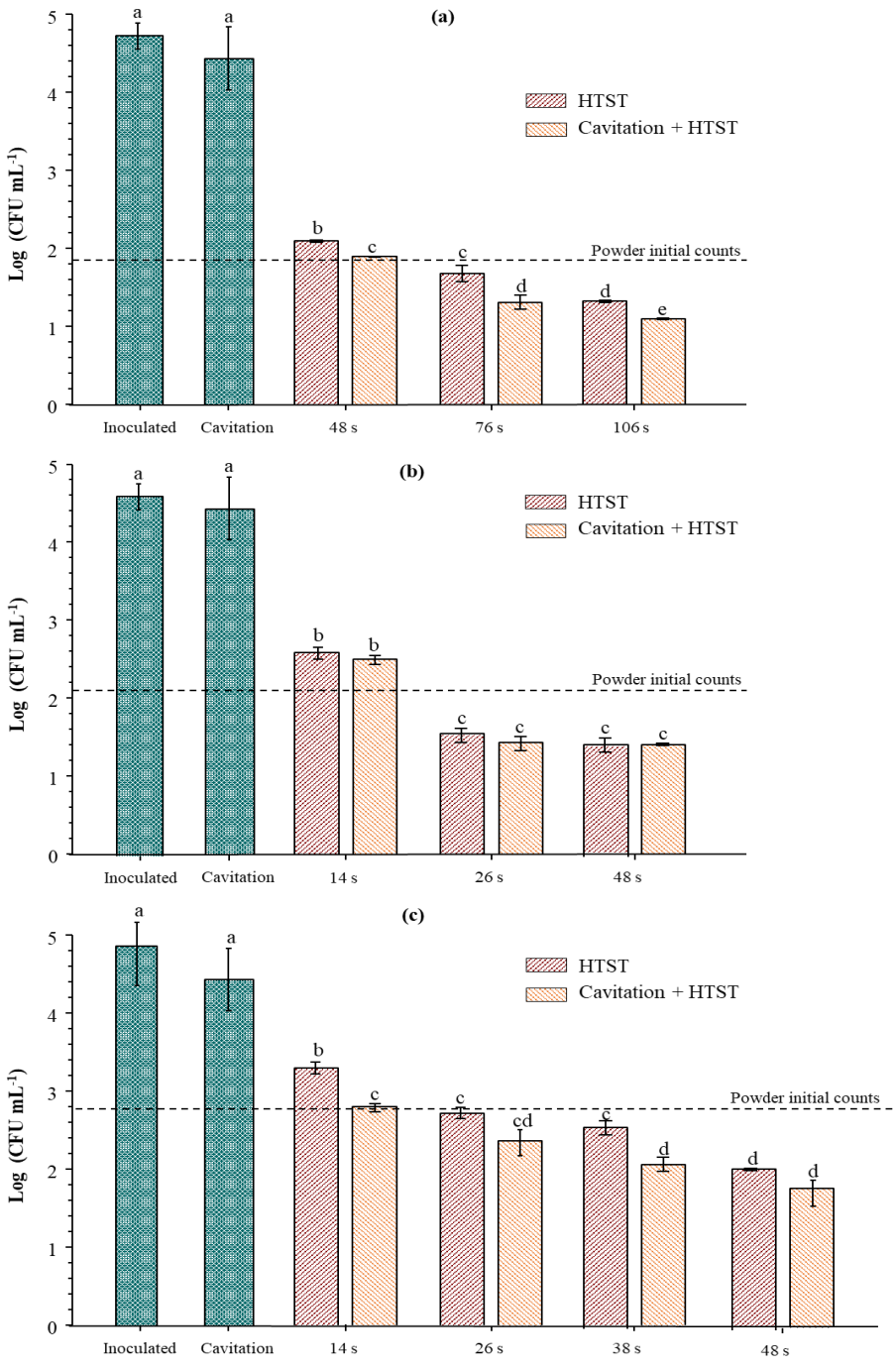

Figure 14. Survival of *B.coagulans* (ACCT 12245) in skim milk concentrate (34-36% total solids) at different points within the experimental rig: after inoculation (feeding tank), after cavitation (3600 RPM), and at: (a) 75, (b) 80, and (c) 85°C. The entire process was performed at 100 L h^{-1}. The discontinuous line represents the initial microbial load of the powder. Mean ± standard deviation within each column with different letters (a–e) are significantly different ($p < 0.05$) according to Tukey test.

Thermal resistance

Figure 15 shows the survival curves for of *B.coagulans* in skim milk concentrate (34-36% total solids). For both processes (HTST and cavitation followed by HTST), visual inspection of the survival curves indicates that the fits obtained are fairly reasonable, and it also evident that the first-order model can be used to represent the kinetics.

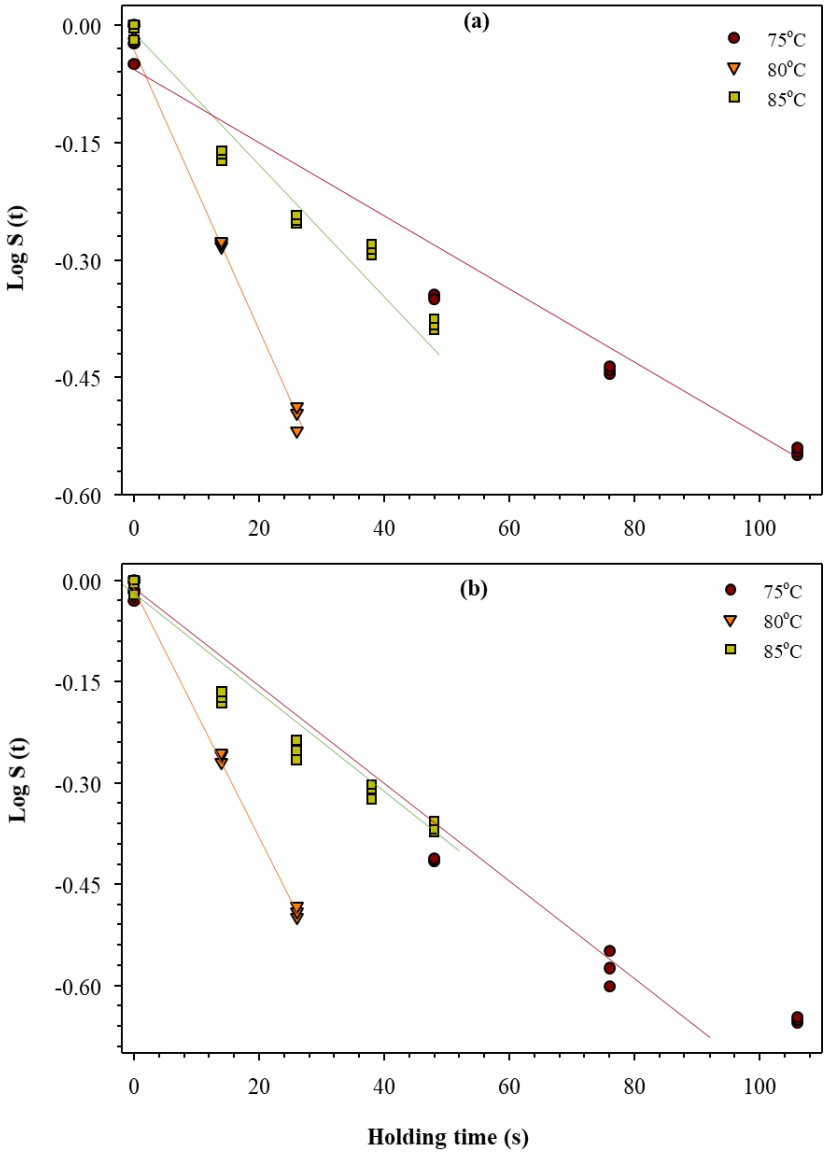

Figure 15. Survivor curves of *B.coagulans* (ACCT 12245) in skim milk concentrate (34-36% total solids) at different temperatures: (a) Hight-Temperature-Short-Time (HTST) and (b) Cavitation followed by Hight-Temperature-Short-Time (HTST).

The experimental data presented in **Figure 15** were fitted using Equation (17) to obtain the associated D values. **Table 3** summarizes the D values for *B.coagulans* at different temperatures obtained after HTST and cavitation followed by HTST.

Table 3. Decimal reduction values for *B.coagulans* (ACCT 12245) in skim milk concentrate (34-36% total solids) at different temperature.

Temperature	**HTST**		**Cavitation+HTST**	
	$\boldsymbol{D}$ **± 95%CI**	$\boldsymbol{R^2}$	$\boldsymbol{D}$ **± 95%CI**	$\boldsymbol{R^2}$
75°C	470 ± 66 s	0.981	375 ± 62 s	0.977
80°C	121 ± 10 s	0.997	125 ± 10 s	0.998
85°C	315 ± 38 s	0.981	320 ± 42 s	0.977

D — Decimal time reduction (s); 95% CI — 95% confidence interval; R^2 — coefficient of determination

The calculated D values were much higher than their respective 95% confidence interval, meaning that these parameters can be used for prediction. Moreover, the R^2 values (>0.970, **Table 3**) indicate that the first-order model can mathematically represent the inactivation of *B.coagulans* within the tested conditions. A closer inspection of the D values reported in **Table 3** reveals that only those values obtained at 75°C showed differences between the processes. For instance, the D value for process that combines cavitation and HTST was lower than that obtained for HTST alone (375 ± 62 and 470 ± 66 s, respectively). Contrary, the D values obtained at 80 and 85°C were similar in magnitude between the two processes (**Table 3**). Another relevant observation is that increasing the temperature from 75 to 80°C showed a considerable reduction in the D value, from 470-375 to 120-125 s. This observation is not surprising since increasing the temperature produces higher inactivation rates, according to the first-order kinetics. However, an increment of 2.5-folds in the calculated D values was observed when the

temperature increased up to 85°C. A possible explanation for such a behavior is the high initial counts found in the powder used for the preparation of skim milk concentrate. Indeed, the powder used for the experiments conducted at 85°C contained 2.94 ± 0.82 log CFU mL^{-1}. In closing, the calculated D values can provide useful information regarding the inactivation kinetic. However, the magnitude and their interpretation should be considered cautiously because of the relatively high number of bacteria in the initial powder.

3.4. Conclusions

A process that combines cavitation and thermal treatment was developed and further characterized. The newly developed process can be operated within a wide range of processing conditions (50-300 L h^{-1}, 600-3600 RPM, 70-85°C with residence time from 10-110 s). A 3.5 log reduction was obtained by cavitation followed by thermal treatment, while thermal treatment along yielded a 2.77 log reduction. Contrary, individual cavitation did not produce any significant reduction. The outcomes of this chapter present opportunities for utilizing cavitation in combination with thermal treatment for inactivating thermoduric sporeformers with a single pass.

3.5. References

Ali, A. K. A., Smith, K. E., Burrington, K. J. & Lucey, J. A. (2013). Microbiological quality of nonfat dry milk and skim milk powder produced in the United States. ADSA Poster T290. Journal of Dairy Science. 96(E-Suppl. 1):101.

Ansari, J. A., Ismail, M., & Farid, M. (2017). Investigation of the use of ultrasonication followed by heat for spore inactivation. Food and Bioproducts Processing, 104:32-39.

Anonymous. (2019). Milk powder market - Global market size, analysis, share, research, business growth and forecast to 2025. Industry Research. Co.

Bawa, D. (2015). Inactivation of thermodynamic sporeformers and spores in skim milk by continuous ultrasonication and hydrodynamic cavitation in combination with thermal treatments. Master theses South Dakota State University.

Buehner, K. P., Anand, S., & Djira, G. D. (2015). Prevalence of thermoduric bacteria and spores in nonfat dry milk powders of Midwest origin. Journal of Dairy Science, 98(5):2861-2866.

Burgess, S. A., Lindsay, D., & Flint, S. H. (2010). Thermophilic bacilli and their importance in dairy processing. International Journal of Food Microbiology, 144(2):215-225.

Dumpler, J., & Kulozik, U. (2016). Heat-induced coagulation of concentrated skim milk heated by direct steam injection. International Dairy Journal, 59:62-71.

Khanal, S. N., Anand, S., Muthukumarappan, K., & Huegli, M. (2014). Inactivation of thermoduric aerobic sporeformers in milk by ultrasonication. Food Control, 37:232-239.

Hill, B. M., & Smythe, B. W. (2012). Endospores of thermophilic bacteria in ingredient milk powders and their significance to the manufacture of sterilized milk products: an industrial perspective. Food Reviews International, 28(3):299-312.

Reich, C., Wenning, M., Dettling, A., Luma, K. E., Scherer, S., & Hinrichs, J. (2017). Thermal resistance of vegetative thermophilic spore forming bacilli in skim milk isolated from dairy environments. Food control, 82:114-120.

Scott, S. A., Brooks, J. D., Rakonjac, J., Walker, K. M. R., & Flint, S. H. (2007). The formation of thermophilic spores during the manufacture of whole milk powder. International Journal of Dairy Technology, 60(2):109-117.

Sharma, A., Jana, A. H., & Chavan, R. S. (2012). Functionality of Milk Powders and Milk-Based Powders for End Use Applications—A Review. Comprehensive Reviews in Food Science and Food Safety, 11(5):518-528.

Walstra, P., Wouters, J. T. M., & Geurts, T. J. (2006). Dairy Science and Technology (Second Edition ed.): CRC Press Taylor & Francis Group.

Wedel, C., Wunsch, A., Wenning, M., Dettling, A., Kayser, K. H., Lehner, W. D., & Hinrichs, J. (2018). Thermal treatment of skim milk concentrates in a novel shear-heating device: Reduction of thermophilic spores and physical properties. Food Research International, 107:19-26.

Chapter 4

Hydrodynamic cavitation: Process opportunities for ice cream formulations

4.1 Introduction

One of the primary focus of the dairy industry is to provide innovative products with natural ingredients by avoiding artificial ingredients or synthetic chemicals. Nowadays, numerous consumers read the lists of ingredients of a given product before they purchase. More importantly, these consumers are willing to pay more for food products that they perceived as natural, familiar, simple, and minimally processed. This is a worldwide movement that is driving many manufacturers to reformulate their original products without compromising on flavor, texture, mouthfeel, and functional properties (Asioli et al., 2017). As a result, there is a proliferation of clean label products already in the market; however, it has also challenged dairy manufactures to explore alternative technologies in order to maintain the desire attributes of foods formulated with fewer ingredients.

Nowadays, the ideal food product of modern consumers would be formulated with perceived healthy ingredients and free of additives. Interestingly, dairy processors have developed a variety of low-fat and low-sugar ice-cream and frozen novelty products, partially addressing the demand for healthy products. Contrary, the removal of undesirable ingredients such as stabilizers from ice-cream is a major challenge from a technological point of view. Industrially, the characteristic flavor, body, and texture of ice-cream is obtained using a variety of processing ingredients/aids (Wahlgren et al.,

2015). Specific details on the manufacture of ice-cream can be found elsewhere (Goff, 2016).

During the manufacture of ice-cream, emulsification and subsequent dispersion of fat droplets within the continuous phase are key processing steps (Walstra, 1993). Such a fine dispersion is kinetically active due to colloidal and hydrodynamic interactions leading to inter-droplet collisions which may results in the formation of larger droplets (McClements, 2004). This is known as coalescence and it is avoided by the addition of water-soluble polymers, called stabilizers. The phenomenon of coalescence has been extensively reviewed elsewhere (Lee et al., 2013; Jafari et al., 2008; Håkansson & Hounslow, 2013). In general, making stable colloidal dispersions requires use of high concentration of surfactants and/or high input of mechanical energy (Martínez-Monteagudo et al., 2017).

In the last decade, consumers oriented with health and wellness life style have perceived synthetic emulsifier agents (stabilizers and thickeners) as undesirable ingredients. Thus, dairy processors are interested in identifying cost-effective technological solutions that improve emulsification and potentially minimize the use of stabilizers. Stabilizers play an essential role in the behavior of ice cream (Goff, 2016). Guar gum, carboxymethyl cellulose, xanthan gum, sodium alginate, and carrageenan are example of stabilizers commonly used for the manufacture of ice-cream. Each ingredient has its own properties, and combinations of two or more stabilizers are used to enhance their overall efficacy. Stabilizers improve emulsion stability to prevent serum separation

and the creaming of fat, stabilize the air bubbles, aid in the suspension of liquid flavor, reduce the growth of lactose crystals, and prevent the migration of free water (Chang & Hartel, 2002). Reducing the concentration of stabilizers can generate undesirable melting properties as well as create a heavy and chewy body. Although stabilizers are key ingredients in ice cream production, some stabilizers have been chemically derivatized to improve their solubility in water, which does not meet consumers' demands for natural and clean ingredients. Often when such target ingredients are simply removed from the formulation, it adversely affects the organoleptic properties of the product, texture and appeal.

Researcher and dairy manufacturers are actively exploring alternatives for reducing the concentration of stabilizers. Strategies currently used are:

1) Optimization of the existed formulations.
2) Substitution of synthetic additives.
3) Application of emerging technological approaches.

Optimization consists of a gradually removal from the formulation until no significant change is perceived by a group of sensory panelists. This strategy has limited success since such compounds are not entirely removed from the formulation. Substitution involves the use of other chemicals, and often requires relatively large concentrations. On the other hand, the application of emerging technologies has been an active area of research. Examples of such technologies are high pressure processing, pulsed electric

fields (PEF), ultrasound, and hydrodynamic cavitation. In this chapter, the feasibility of using hydrodynamic cavitation for improving the emulsification of ice-cream mix was evaluated. The feasibility was judged in terms of particle size and rheology measurements (strain sweep, frequency sweep, and flow curve of the ice-cream mix).

4.2 Materials and Methods

Preparation of ice cream mix preparation

An ICM of industrial interest was used to assess the feasibility of HC for reducing the concentration of stabilizers. The formulation of ICM consisted of 38.4% of raw cream (Davis Dairy Plant at South Dakota State University, Brookings, SD), 37.1% of skim milk (Davis Dairy Plant), 6.1% of non-fat dry milk (Continental Dairy Facilities, LLC, Coopersville, MI), 14.8 of granulated sugar (United Sugar Corp., Minneapolis, MN), 3.3% of dry corn syrup (Cerestar USA, Inc., Hammond, IN), and 0.28% of blend of stabilizers (Continental Colloids, Inc., West Chicago, IL). The blend of stabilizers consisted of guar gum, locust bean gum, carrageenan, polysorbate 80, and mono- and diglycerides. The dry ingredients were dissolved in skim milk, and blended using an industrial blender (Breddo likwifier, Kansas City, MO) operated at 1,755 RPM for 15min at room temperature.

Processing treatments

Three sets of experiments were performed to select the processing conditions of the rotational cavitation. Study 1 consisted on the evaluation of HC on the particle size of raw cream. Fresh cream (36-38% fat) obtained from the Davis Dairy Plant (Brookings,

SD) was adjusted with skim milk to obtain a final concentration of 13%, which represents the fat content found in the ICM. The adjusted cream was stored overnight at 4°C before further treatment. Then, the cream was treated at nine different rotor speed-flow rate combinations (2400-3600 rpm and 50-200 L h^{-1}) using a rotational HC from SPX Flow Technology, previously described in chapter 2. In study 2, the ICM was treated at five different rotor speed-flow rate combinations (2400-3600 RPM and 100-200 L h^{-1}). At the end of the treatment, the samples were analyzed for particle size and rheological behavior. An ICM was manufactured with conventional homogenization and heat treatment (HTST, 75°C for 15 s), and it was used as a control. Study 3 evaluated the combined effect of HC on the properties of ICM formulated with reduced stabilizers (0.28, 0.21, 0.14, and 0%). Each experimental run cosisted of 10 L of ICM. All experiments were performed in triplicate. The statistical analysis was conducted using Sigmaplot software V11 for windows (SPSS Inc., Chicago, IL, USA).

Particle size distribution

The distribution of particles was determined by laser diffraction method using a Horiba LA-920 static light (Horiba Scientific, Kyoto, Japan). Deionized water was used as the diluent, and the relative refractive index was set at 1.14, calculated as the refractive index of the particle (1.52 for milk fat) divided by the refractive index of the diluent (1.33 for water). Drops of either cream or ICM was added into the chamber until transmittance equilibrated between 70 and 95%. The temperature was maintained between 40 and 45°C to ensure the milk fat was in a liquid state. For each sample, size distribution was obtained in percentage of volume as function of droplet diameter in the range of 0.01-

4500 μm. The size distribution histogram was analyzed with polydisperse analysis to calculate mean droplet diameter and percentiles.

Dynamic rheological measurement

The dynamic rheological behavior of the treated samples was analyzed in an MCR92 rotational rheometer (Anton Paar USA, Inc. Vernon Hills, IL) equipped with cup-bob configuration (60 mm bob and 120 mm cup geometry). Samples were tested at 4°C, and 37 data point were collected. The rheological behavior of the ICM was determined by the strain sweep and frequency sweeps. The strain sweep was first conducted in order to determine the linear viscoelastic (LVE) region. Then, the frequency sweep was performed at a constant shear strain, a value within the LVE region, with a frequency range of 0.1 to 10 Hz. The complex shear module (G*) was acquired using the rheometer software, while the storage module (G') and the loss module (G") were calculated according to Equation (18) and (19).

Equation (18)

$$G' = G^* \cdot \cos\delta$$

Equation (19)

$$G^{"} = G^* \cdot \sin\delta$$

Steady shear measurements

The flow curve of the ICM was determined in an MCR92 rotational rheometer (Anton Paar USA). The measurements were carried out in the shear rate range of 1- 100s^{-}

[1] at 4℃. The Ostwald de Waele model was used to determine flow behaviors of the sample, according to Equation (20).

Equation (20)

$$\sigma = K \cdot \dot{\gamma}^n$$

Where σ is shear stress, K is the consistency coefficient, $\dot{\gamma}$ is the shear rate, and n is the flow behavior index.

4.3 Results and Discussions

Study 1: Effect of cavitation on particle size distribution on raw cream

Figure16 shows the effect of HC on the particle size distribution of raw cream (13% fat). The untreated cream showed two distinguishable peaks of different broadness that spanned from 200 to 70 μm and 17 to 2 μm, respectively. The peak associated to larger particles accounted for about 27% of the total particles in raw cream, while the smaller peak accounted for the remaining 73%. Such a bimodal distribution of particles for untreated cream is not surprising. Similarly, Amador-Espejo et al. (2014) reported a bimodal distribution for untreated milk. In general, the application of hydrodynamic cavitation shifted the distribution of particles towards a single peak of different broadness. The spanned of each peak showed to be dependent of the speed of the rotor.

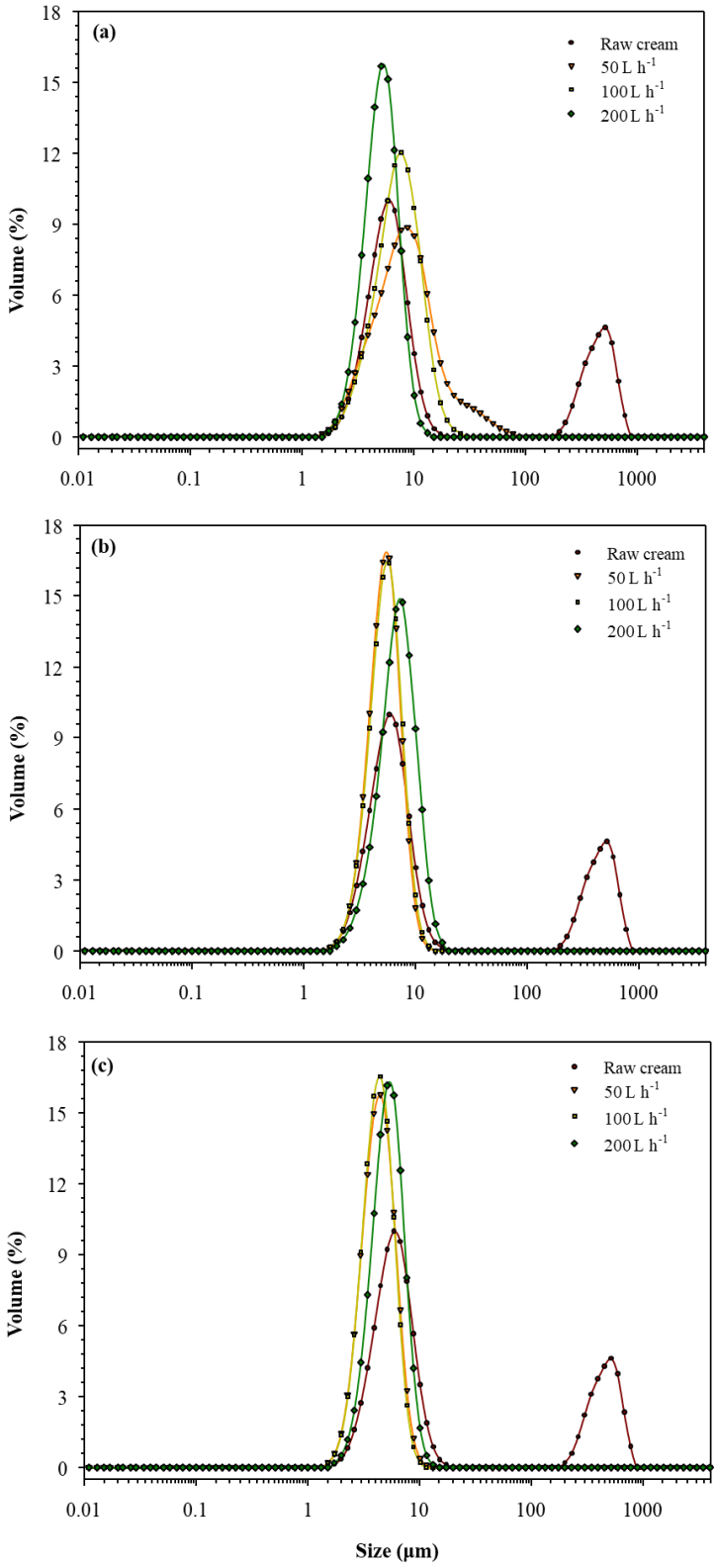

Figure 16. Effect of speed of the rotor on the particle size distribution of raw cream (13% fat): (a) 2400 RPM; (b) 3000 RPM; and (c) 3600 RPM.

At a speed of the rotor of 2400 RPM (**Figure 16a**), the peak spanned from 1.5 to 77, 1.7 to 13, and 1.5 to 11 μm for 50, 100, and 200 L h^{-1}, respectively. Similar behavior was observed when the speed of the rotor increased to 3000 RPM (**Figure 16b**), where the peak spanned from 1.7 to 26, 1.7 to 13, and 1.5 to 10 μm for 50, 100, and 200 L h^{-1}, respectively. Further increase of the speed of the rotor did not significantly change the broadness of the peak. For instance, at 3600 RPM (**Figure 16c**), the distribution of particles spanned from 1.7 to 13, 2 to 17, and 1.7 to 13 μm for 50, 100, and 200 L h^{-1}, respectively. The information presented in **Figure 16** suggests that the application of hydrodynamic cavitation at 3000-3600 RPM resulted in similar distribution of particles regardless of the flow rate.

Study 2: Effect of cavitation on ice cream mix

Figure 17 illustrates the effect of hydrodynamic cavitation on the particle size distribution of the ice cream mix. For comparison, the particle size distribution of ice cream mix conventionally homogenized (two-stage homogenization in a Gaulin type homogenizer) is included in **Figure 17**, and it was denominated as commercial sample. The lowest distribution of particles was obtained in the commercial ICM, where two overlapped peaks were observed, spanning from about 10 to 0.1 μm. Both peaks showed a maximum size at about 6% of volume distribution (0.17 and 0.51 μm, respectively). In the case of ICM treated with cavitation, the curves showed a single peak of similar broadness that ranges from 45.6 to 1.4, 17.3 to 1.3, 14.5 to 1.2, 17.4 to 1.5 μm for 2400 RPM at 100 L h^{-1}, 3000 RPM at 100 L h^{-1}, 3600 RPM at 100 L h^{-1}, and 3600 RPM at 200 L h^{-1}, respectively. In addition, the cavitated samples yielded at maximum size between

10-11% of volume distribution at 3.3-5.8 μm. Interestingly, the largest particle size distribution was obtained at 3000 RPM with 100 L h^{-1}. For the cream, this process condition allowed ice cream mix to reduce the fat globule size, however, it increased the particle size in the ice cream mix processing. The particle size distribution plays a major role during the manufacture of ice cream. Previous studies reported that the size of the fat globule and its distribution affected the melting rate of frozen desserts (Muse & Hartel, 2004). Muse & Hartel (2004) reported that when fat globule size was below a median value of 0.85 μm.

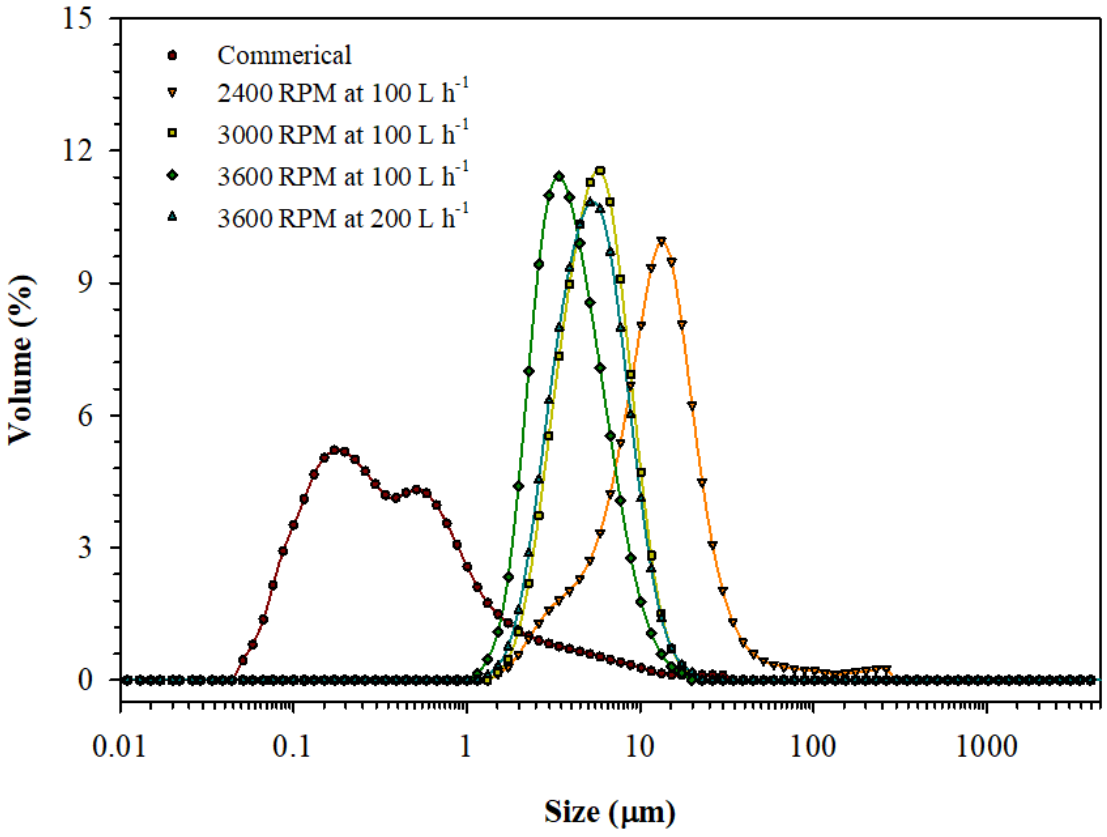

Figure 17. Particle size distribution of ice cream mix treated with hydrodynamic cavitation.

Figure 18 show the storage module (G') as a function of strain amplitude for different samples of ice cream mixes. The strain sweep of ICM mixes was performed to determine the linear viscoelastic region (LVR), where G' was constant with increasing strain. The LVR indicates the range of shear strain at which the test sample behave without destruction of its structure. Outside the LVR, the test samples structure starts to disrupt, and the values of G' decreases with increasing strain. The G' represents the elastic properties of the products that can be seen as solid-state behavior, while $G^{"}$ represents the viscous properties of the sample, which can be seen as liquid-state behavior of products were also obtained from strain sweep test.

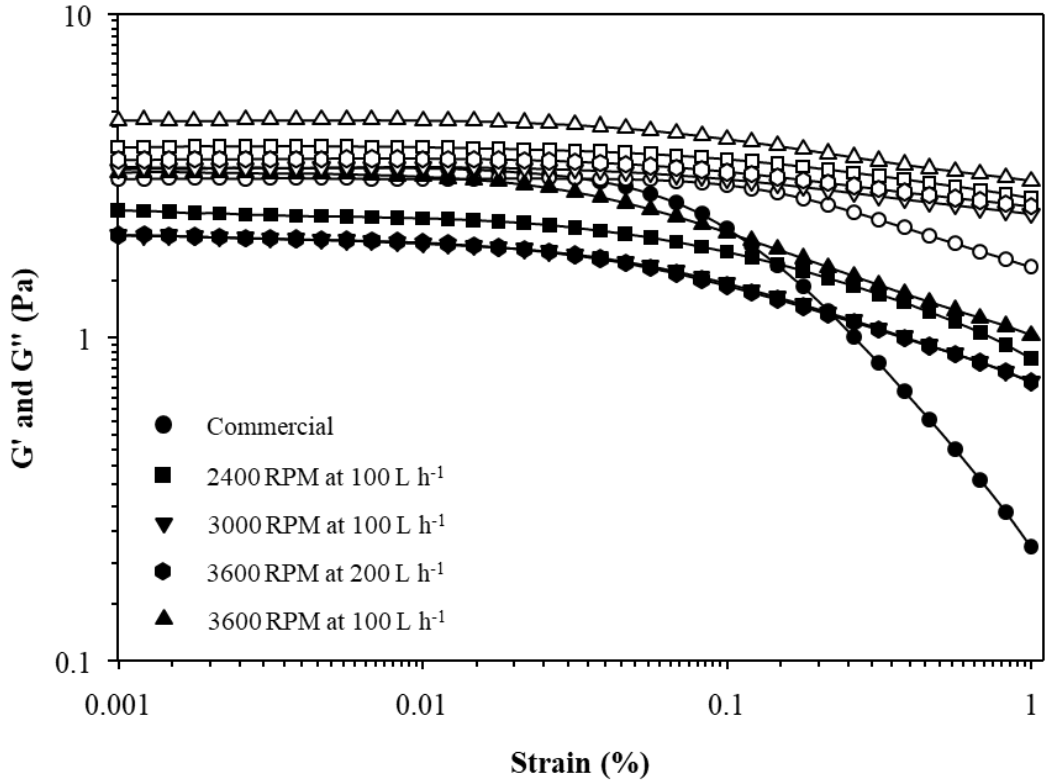

Figure 18. Strain sweep of different ice cream mixes. Frequency = 10 rad s^{-1}. Open symbols correspond to storage module (G'), and closed symbols represent loss module ($G^{"}$).

The commercial ICM showed a viscoelastic region within the range of 0.1 to 7%, where G'>G''. This observation indicates that within the LVE region, the commercial ICM behaved like gel-like or structured solid, known as viscoelastic solid material. On the other hand, ICM treated with cavitation displayed a behavior where G'>G''. An interpretation of such observation is the sample consisted of different structures in which the particles are connected through chemical bonds (Hesarinejad et al., 2014). **Figure 18** also shows the yield point and flow point. The yield point also known as the end of the LVR region and solid structure (G') starts to deform. The flow point is the value of shear stress at the cross over point (G'=G'') at which the sample behaves like liquid. Overall, viscoelastic liquids are mainly consisted of unlined individual molecules without chemically crosslinked. The commercial ICM displayed a yield point and a flow point at shear strain of approximately 6%. On the other hand, the samples treated with HC displayed a fluid state across the entire deformation range. The cavitated ICM displayed the ability to flow from 0.1% shear strain, and their respective yield point was obtained from shear strain at approximately 5%.

The information obtained from the strain sweep analysis was further used to define the limits of the viscoelastic region and determine the mechanical spectra of the ICM. Frequency sweep plots are commonly used to characterize the mechanical spectra of emulsified foods (Steffe, 1996). Frequency sweep test of ICM sample was carried out at 0.5% shear strain which correspond within the viscoelastic region (**Figure 19**).

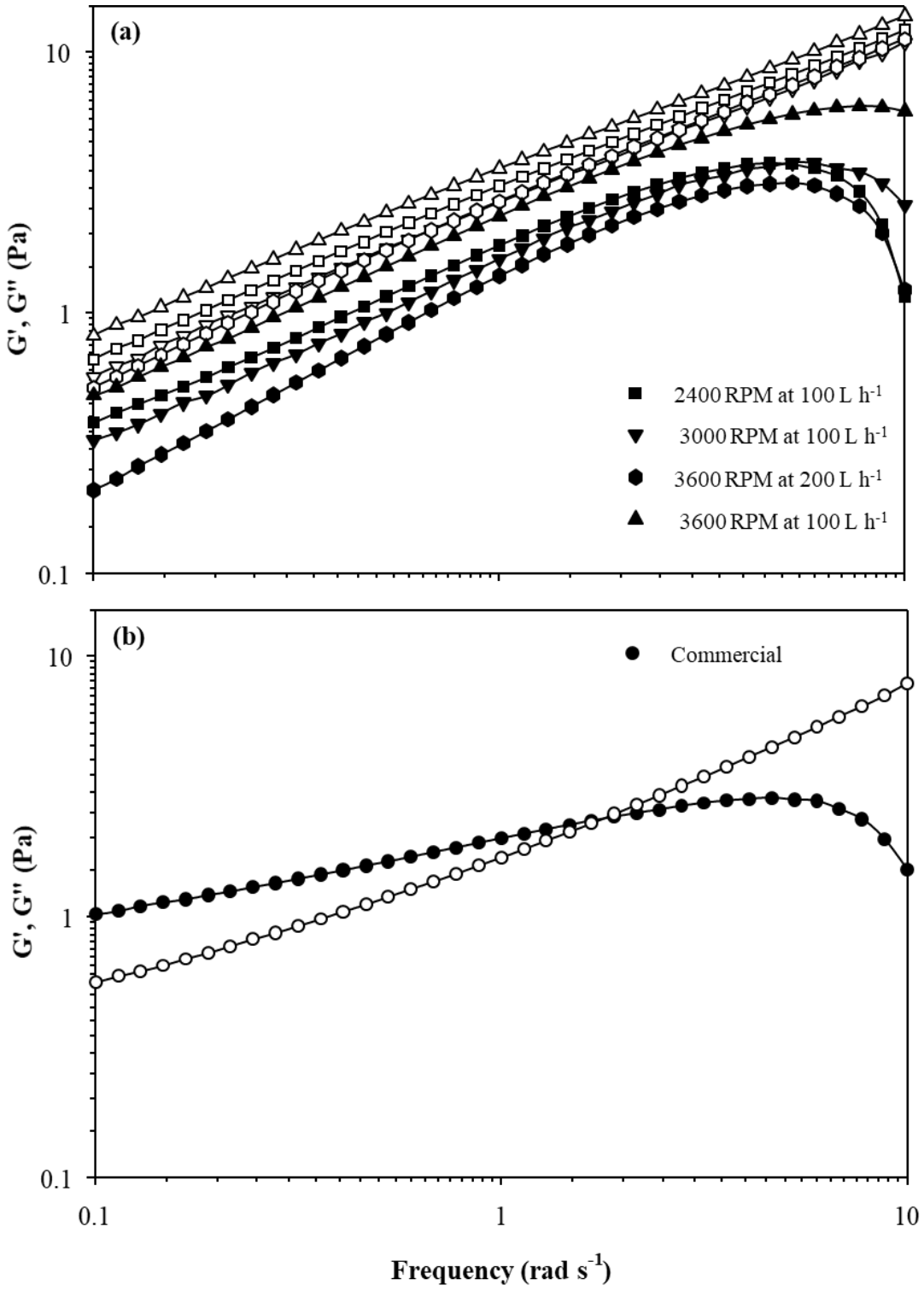

Figure 19. Frequency sweep analysis for ice cream mixes: (a) cavitated samples, and (b) commercial ice cream mix. Strain = 0.5%. Open symbols correspond to storage module (G'), and closed symbols represent loss module ($G^{"}$).

Figure 19a shows the storage module (G') and loss module (G'') as a function of frequency for ice cream mixes treated with hydrodynamic cavitation. The mechanical spectra of ICM treated with hydrodynamic cavitation showed that the G" was higher than G' within the frequency range of 0.1 to 10Hz. These results indicated that ICM samples are susceptible to segregation and particle sedimentation over a long-term storage. Long term storage behavior of dispersed systems can be was evaluated through the mechanical spectra at the lower frequency range (Steffe, 1996). The commercial ICM had a typical behavior of dilute solution, where G' and G" slightly increased with the frequency and G" was higher than G' from 0.1 to 1.6 rad s^{-1}, meaning that the viscous behavior dominates (Paraskevopoulou et al., 2013). Another interpretation of such observation is that the ICM showed physical stability.

The shear stress and shear rate of the different ice cream mixes are shown in **Figure 20**. All curves showed shear thinning behavior, which is a typical behavior for ice cream mix (Kuş et al., 2005; Goff et al., 1994). At a lower shear rate, the molecules are spread out without any order, which resulted in higher viscosity and lower shear stress. However, increased shear rate arranged the molecules in systematic way and this led to decreases in viscosity and higher shear stress. ICM sample treated with cavitation obtained higher apparent viscosity than reference ICM sample. Samples containing larger molecules tend to have a higher viscosity. The large molecules have stronger intermolecular forces attracting them to one another, and there is a greater strength that hinders molecular flow, which results in more viscous products (Pon et al., 2015).

Overall, the cavitation treatment significantly increased the viscosity of the ice cream mix, and the highest viscosity was obtained at 3600 rpm with 100Lh^{-1}.

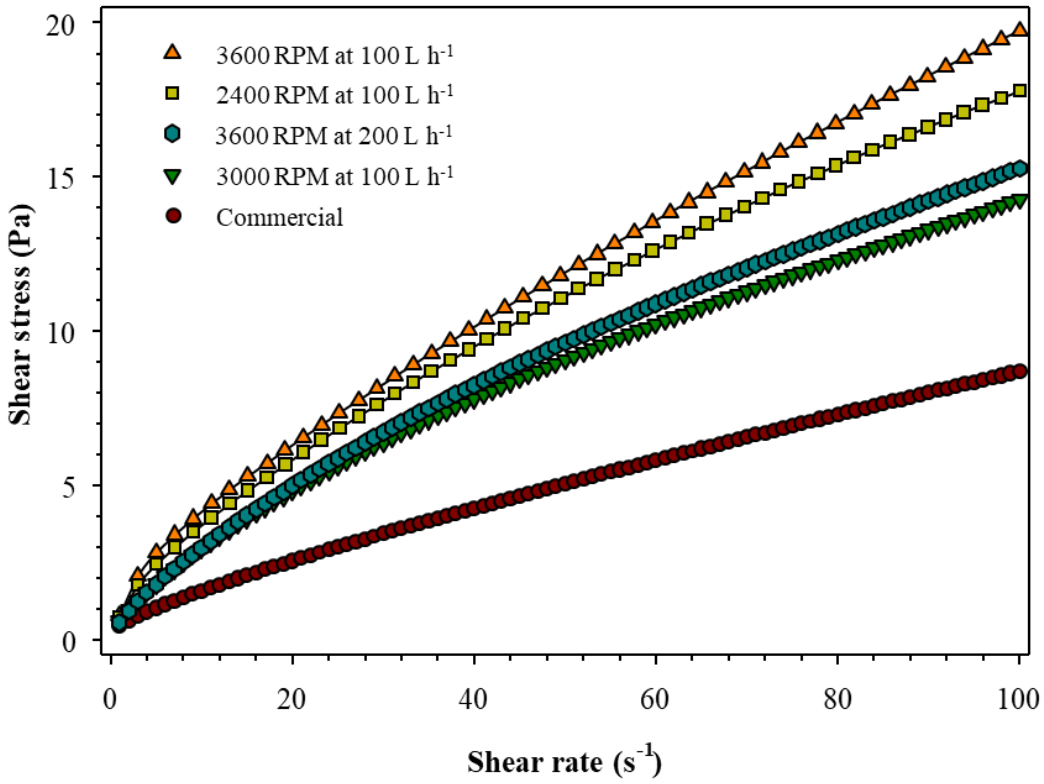

Figure 20. Flow curve of ice cream mix at different processing conditions.

Study 3: reduction of stabilizer

The dynamic rheological measurements (strain and frequency sweeps) of ICM indicated increased product stability with rotation speed of 3600 RPM at a flow of 100 L $^{-1}$. However, the HC also induced significant changes in the mechanical spectra of the ICM. Thus, the processing conditions of 3600 RPM at a flow of 100 L $^{-1}$ was chosen to evaluate the feasibility of reducing the concentration stabilizers. The blend of stabilizers was reduced in the ICM by adding 0.28 (full formulation), 0.21, 0.14, and 0% of the blend. t

Figure 21 shows the particle size distribution of ICM with reduced stabilizer. For comparison the particle size distribution of the ICM conventionally manufactured was included (two-stage homogenization). The removal of stabilizer consistent and systematic shift the distribution of particles towards a bimodal distribution, where two peaks of similar broadness were obtained and they spanned from 652 to 120 μm and from 15 to 1 μm, respectively. Contrary, the ICM added with stabilizers (0.28%) displayed a single distribution peak of particles. Stabilizers are added to ice cream mix to increase the viscosity, prevent separation, delay the growth of crystals. All these functions are closely related to the particle size induced during the handling of the mix.

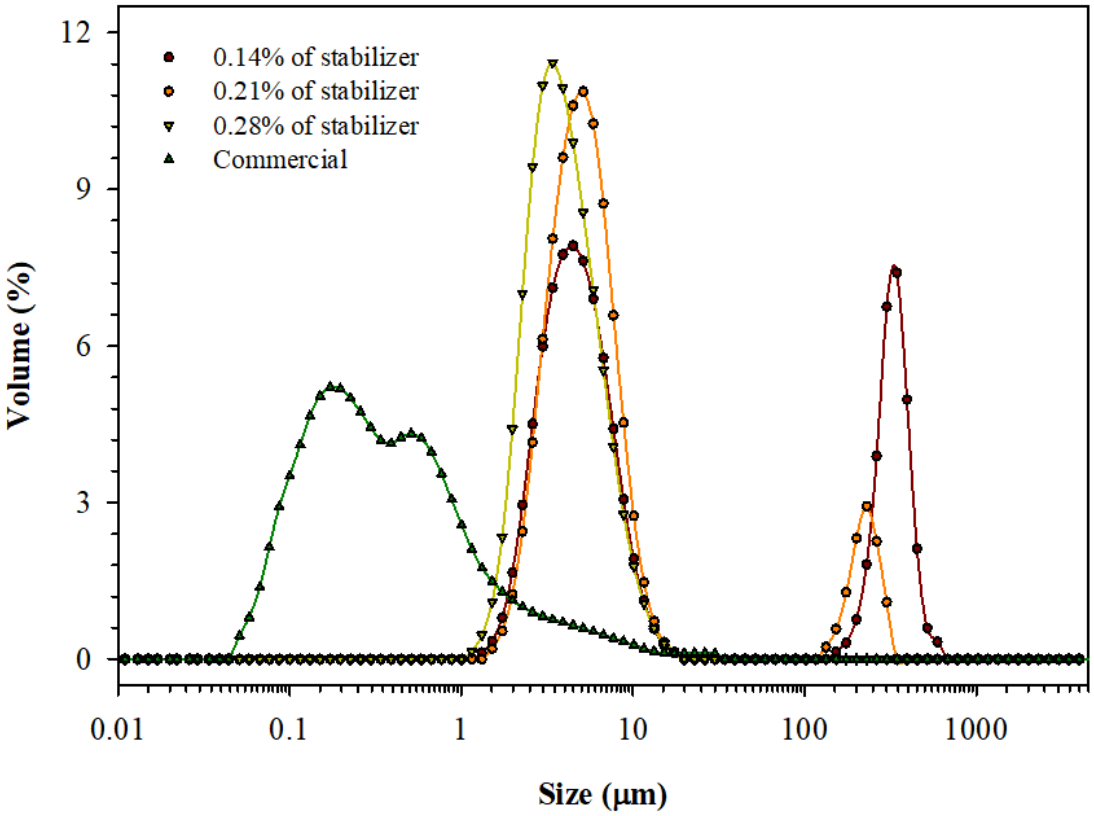

Figure 21. Particle size distribution of ice cream mix formulated with reduced stabilizer. Cavitated samples were treated at 3600 RPM at 100 L h^{-1}.

Figure 22 shows the strain sweep for the ice cream mix formulated with reduced stabilizer and treated at 3600 RPM at 100 L h^{-1}. All the ICM samples were obtained higher G' value than G'' through the shear strain 0.1 to 100%. This indicated that ICM behaved like a viscoelastic liquid, and the flow point started from shear strain 0.1%.

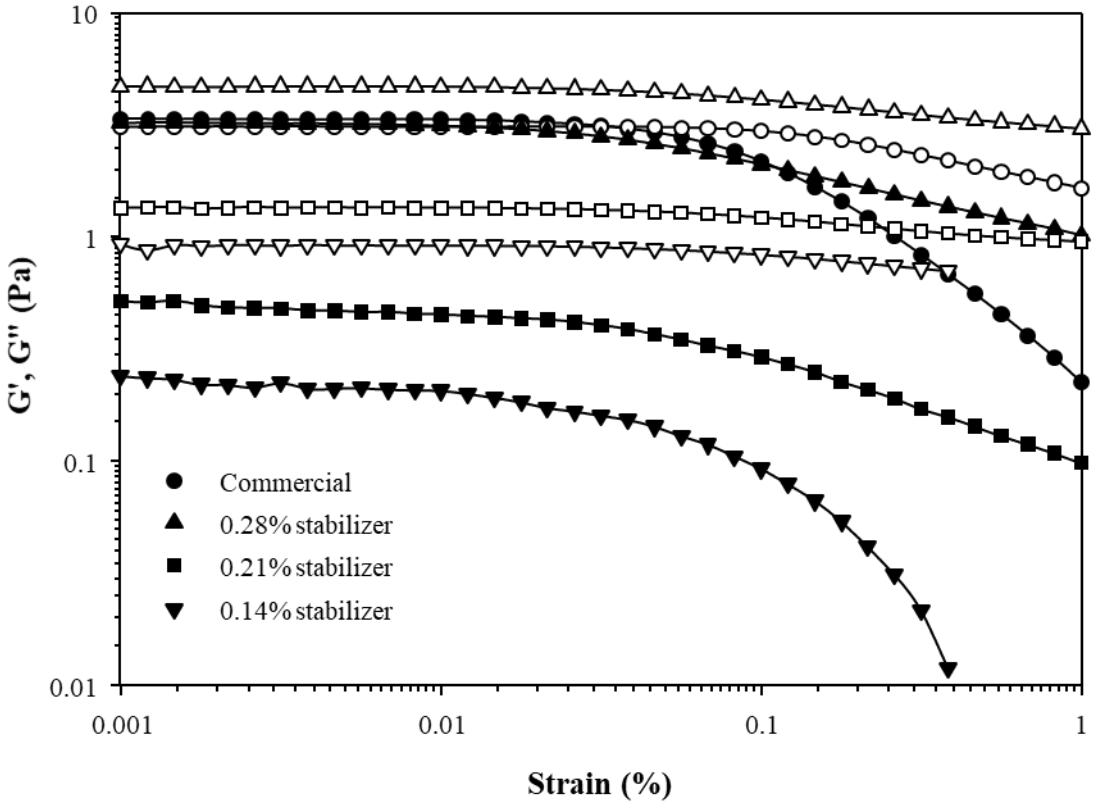

Figure 22. Strain sweep analysis of ice cream mix formulated with reduced stabilizer. Ice cream mixes were manufactured at 3600 RPM at 100 L h^{-1}. Frequency = 10 rad s-1. Open symbols correspond to storage module (G'), and closed symbols represent loss module ($G^{"}$).

The ICM with 0% stabilizer showed as the ideally viscous behavior and phase shift angle (δ) was obtained 90◦ with G' is close to 0. This observation indicates that no elastic portion existed in the ICM. When the phase shift angle was obtained between 45 to 90◦, the sample is viscoelastic liquid and when the value is close to 90◦, the sample has more

viscous behavior. When the phase shift angle was obtained between 0 to 45◦, the sample is viscoelastic solids and then the value is close to 0◦, the sample becomes to behave ideally elastic behavior without viscous portion. The ICM added with 0.21% stabilizer was obtained phase shift angle from 68 to 84◦, and ICM with 0.14% stabilizer was obtained phase shift angle from 77 to 90◦, ICM with 0.28% stabilizer had 55 to 70◦. The results indicated that by reducing the stabilizer amount ICM behave like ideally viscous product by losing elastic portion.

Figure 23 shows the mechanical spectra of the ICM formulated with reduced stabilizer. All the ICM samples showed G”>G’ under the measuring conditions from 0.1 to 10Hz. Higher G’ value was obtained from ICM with 0.28% stabilizer. G’ value decreased when stabilizer amount was decreased in ICM samples. The results indicated that reducing the stabilizer amount resulted in lowering stiffness of ICM sample and allowed more viscos portion by losing its elastic portion.

The viscosity obtained for ICM formulated with reduced stabilizer is given in **Figure 24**. In order to understand ICM viscosity from different processing condition, viscosity was measure at shear rate of 1, 13, and 100 s^{-1}. Shear rate 1 indicates that the product is in the rest status, and shear rate 13 s^{-1} represent the condition when products flow through the processing pipe-line and 100 s^{-1} indicates that the products encounter the centrifugal pump condition. Higher viscosity was obtained from ICM with 0.28% stabilizer and low viscosity was obtained with ICM with 0% stabilizer from each shear rate.

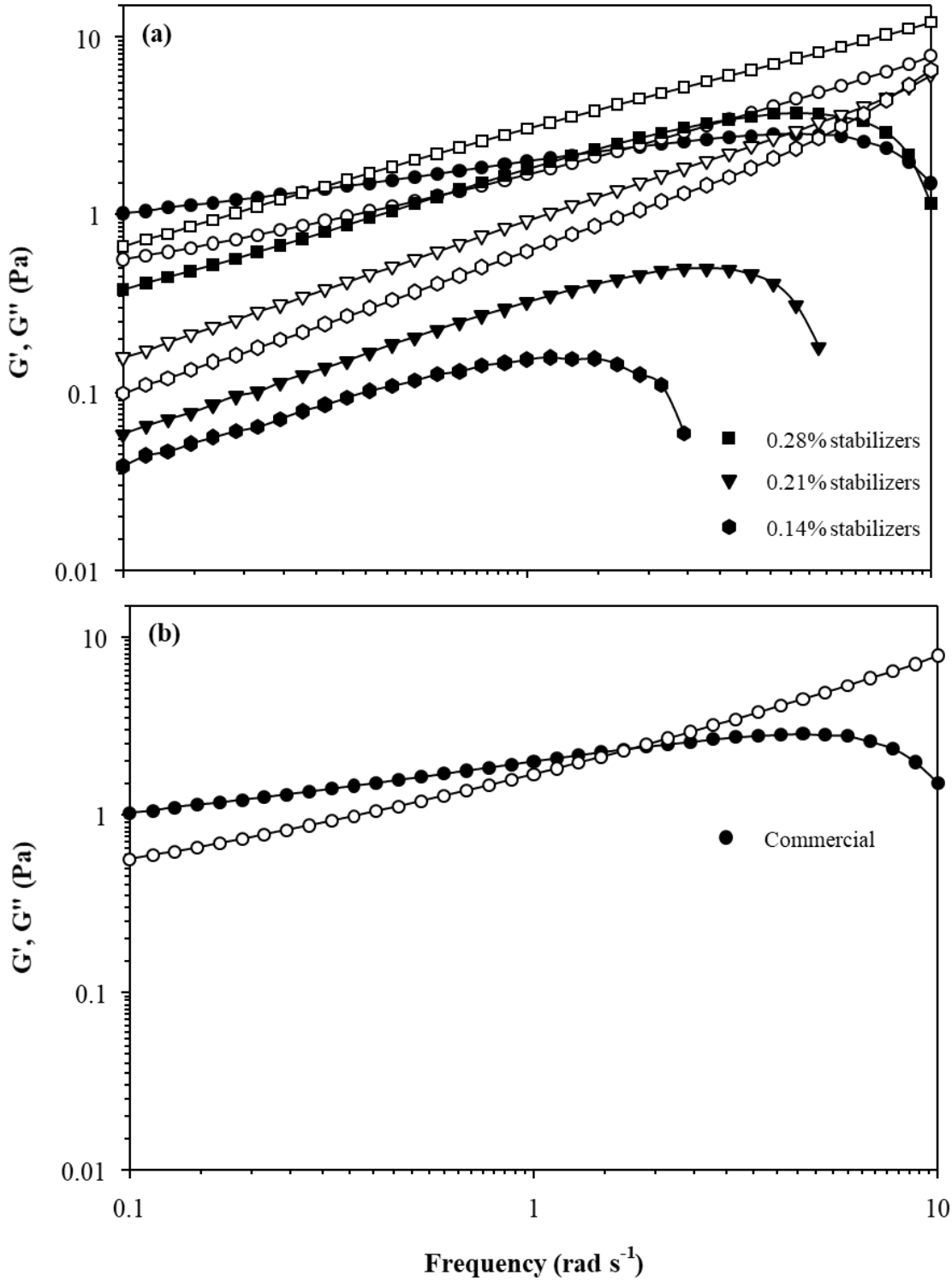

Figure 23. Mechanical spectra of the ice cream mix formulated with reduced stabilizer. Samples were manufactured at 3600 RPM at 100 L h^{-1}. Strain = 0.5%. Open symbols correspond to storage module (G'), and closed symbols represent loss module ($G^{"}$).

The results indicate that viscosity be proportionate to stabilizer amount. This increased viscosity could have influenced by decreased whipping abilities. The previous study in whipped creams demonstrate that use of whipped cream resulted in increased viscosities by leading to lower overruns impact but higher stability (Goff et al., 1994). High viscosity systems allowed to foam stability but not favor foaming capacity.

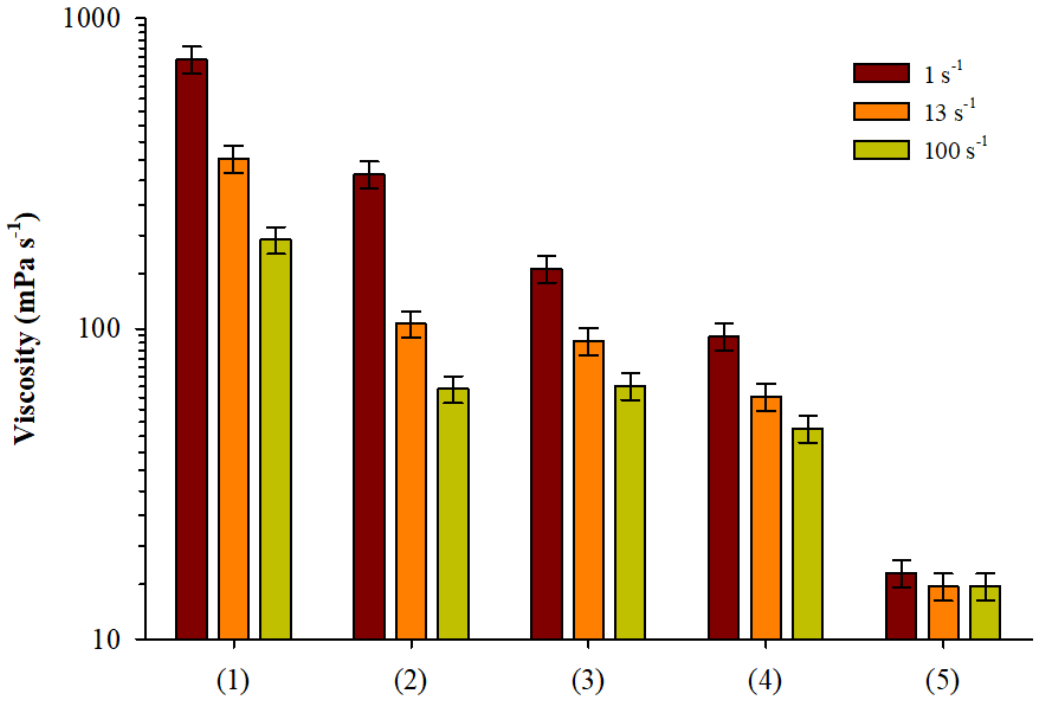

Figure 24. Changes in the viscosity of ice cream mix formulated with reduced stabilizer. The cavitated samples were manufactured at 3600 RPM at 100 L h^{-1}. (1) mix formulated with 0.28% of stabilizer; (2) commercial mix with 0.28%; (3) mix formulated with 0.21% of stabilizer; (4) mix formulated with 0.14% of stabilizer; and (5) mix formulated with 0% of stabilizer.

The application of HC significantly increased the viscosity of the mix, and such changes were more notorious at low shear spectrum. For instance, in the low shear spectrum (1 s^{-1}), HC yielded an increase in the viscosity up to 1.6-fold. Contrary, at

higher shear rates (up to 13 s^{-1}), the increase in viscosity was even more pronounced, up to 2.41-fold. These observations exemplify the complexity of interactions between different ingredients during HC. This is an important consideration in relation to process engineering since changes in the viscosity might alter the processing conditions as well as the final quality of the product.

4.4. Conclusion

Hydrodynamic cavitation was applied for the clean label approach in ice cream mix. Particle size of ice cream mix and rheology test was conducted to determine the influence of the stabilizer amounts in ice cream mix. Hydrodynamic cavitation itself reduced the particle size of cream and ice cream mix. Dynamic rheological measurements (strain and frequency sweeps) of ICM indicated increased product stability with rotation speed of 3600 RPM and a flow of 100 L^{-1}. However, the mechanical spectra were considerable different. Imparted viscosities at medium shear rates were at least 2-fold greater compared to formulations homogenized conventionally.

4.5. References

Asioli, D., Aschemann-Witzel, J., Caputo, V., Vecchio, R., Annunziata, A., Næs, T., & Varela, P. (2017). Making sense of the “clean label” trends: A review of consumer food choice behavior and discussion of industry implications. Food Research International, 99:58-71.

Amador-Espejo, G. G., Suàrez-Berencia, A., Juan, B., Bárcenas, M. E., & Trujillo, A. J. (2014). Effect of moderate inlet temperatures in ultra-high-pressure

homogenization treatments on physicochemical and sensory characteristics of milk. Journal of Dairy Science, 97(2):659-671.

Chang, Y., & Hartel, R. W. (2002). Stability of air cells in ice cream during hardening and storage. Journal of Food Engineering, 55(1):59-70.

Goff, H. D., Davidson, V. J., & Cappi, E. (1994). Viscosity of ice cream mix at pasteurization temperatures. Journal of Dairy Science, 77(8):2207-2213.

Goff, H. D. (2016). Ice cream and frozen desserts: Manufacture. Reference Module in Food Science, Elsevier.

Håkansson, A., & Hounslow, M. J. (2013). Simultaneous determination of fragmentation and coalescence rates during pilot-scale high-pressure homogenization. Journal of Food Engineering, 116(1):7-13.

Hesarinejad, M. A., Koocheki, A., & Razavi, S. M. A. (2014). Dynamic rheological properties of Lepidium perfoliatum seed gum: effect of concentration, temperature and heating/cooling rate. Food Hydrocolloids, 35:583-589.

Jafari, S. M., Assadpoor, E., He, Y., & Bhandari, B. (2008). Re-coalescence of emulsion droplets during high-energy emulsification. Food hydrocolloids, 22(7):1191-1202.

Kuş, S., Altan, A., & Kaya, A. (2005). Rheological behavior and time-dependent characterization of ice cream mix with different salep content. Journal of Texture Studies, 36(3):273-288.

Lee, L. L., Niknafs, N., Hancocks, R. D., & Norton, I. T. (2013). Emulsification: Mechanistic understanding. Trends in Food Science & Technology, 31(1):72-78.

Martínez-Monteagudo, S. I., Kamat, S., Patel, N., Konuklar, G., Rangavajla, N., & Balasubramaniam, V. M. (2017). Improvements in emulsion stability of dairy

beverages treated by high pressure homogenization: A pilot-scale feasibility study. Journal of Food Engineering, 193:42-52.

Muse, M. R., & Hartel, R. W. (2004). Ice cream structural elements that affect melting rate and hardness. Journal of Dairy Science, 87(1):1-10.

McClements, D.J. (2004) Food emulsions: principles, practices, and techniques. CRC press, Boca Raton, Florida.

Paraskevopoulou, A., Tsioga, E., Biliaderis, C. G., & Kiosseoglou, V. (2013). Acid-induced gelation of aqueous WPI–CMC solutions: Effect on orange oil aroma compounds retention. Food hydrocolloids, 30(1):368-374.

Pon, S. Y., Lee, W. J., & Chong, G. H. (2015). Textural and rheological properties of stevia ice cream. International Food Research Journal, 22(4):1544.

Steffe, J. F. (1996). Rheological methods in food process engineering. Second Edition. Freeman Press, East Lansing, MI, USA.

Wahlgren, M., Bergenstahl, B., Nilsson, L., Rayner, M., 2015. Formulation of emulsions. In: Rayner, M., Dejmek, P. (Eds.), Engineering Aspects of Food Emulsification and Homogenization. CRC Press Taylor & Francis Group, Boca Raton, Fl, pp. 51-100.

Walstra, P. (1993). Principles of emulsion formation. Chemical Engineering Science, 48(2):333-349.

Chapter 5

Overall conclusions and recommendations

5.1. Overall conclusions

The application of hydrodynamic cavitation for dairy manufacturing is now a commercial reality. Today, the applicability of hydrodynamic cavitation in dairy manufacturing include microbial inactivation, mixing, dispersion, emulsification, and particle size reduction. Intelligent combination of flow rate, speed of rotor, and food formulation offer potential in terms of improving functionality and quality.

The technological solution developed in part through this research can help US equipment vendors to design and commercialize advanced pasteurization concepts that can be used for producing shelf stable and/or extended shelf life products. The study can also help US manufacturers remain competitive in the global market place.

5.2. Recommendations

Recently, there is an increasing growing interest in the development of new technologies r not only for the preservation of foods but also to improve the final quality. Currently, there is only limited efforts in investing the effects of cavitation on product quality. The emerging nature of the hydrodynamic cavitation makes very difficult to compare results from the different studies generated using different configurations. Research efforts are needed to determine the role and their relationship of the mechanical forces acting on a given configuration on the quality, nutrition, and microbial safety. The analysis of the cavitation parameters needs to be studied in more depth through

computational fluid dynamics. Concomitantly, the development of models for simulating cavitating flow should be validated with experimental observation, such as visualization of cavitation bubbles within a flow and acoustical measurements.

Research efforts must be directed towards the inactivation kinetics of thermoduric bacteria. Further development of the hydrodynamic cavitation should also include other microorganisms. The residence time distribution of different fluids needs careful characterization as well as the evaluation of process uniformity. The processing conditions at which a desirable log reduction level has been achieved need to be correlated with quality parameters, such as Whey Protein Nitrogen Index (WPNI). The functional properties of the resulting powder need to be evaluated to further evaluate the feasibility of the hydrodynamic cavitation.

Hydrodynamic cavitation can be used to perform emulsification of ice cream mix. The ice cream mix treated with cavitation displayed higher viscosity, and the impact of freezing on a viscous mix needs further evaluation. The understanding of the changes induced by cavitation on the ice cream mix will help to determine the freezing conditions, and the resulting ice cream should be evaluated using a battery of tests, including composition, rheological properties, microstructure, particle size, hardness, and melting rate.